Journal of Applied Fluid Mechanics, Vol. 18, No. 4, pp. 1064-1085, 2025.
Available online at www.jafmonline.net, ISSN 1735-3572, EISSN 1735-3645.
https://doi.org/10.47176/jafm.18.4.2877

Effect of Motor Blockage on Transient Characteristics of Asymmetric Flow in a Double-suction Centrifugal Fan

S. Du [1], X. Wu [2], Z. Wang [2], W. Yang [2], Z. Yang [3], Z. Wang [1] and W. Zhang [1†]

[1] *Zhejiang Key Laboratory of Multiflow and Fluid Machinery, Zhejiang Sci-Tech University, Hangzhou, Zhejiang 310018, China*
[2] *Zhejiang Yilida Ventilator Co., Ltd., Taizhou, Zhejiang 318056, China*
[3] *Zhejiang Supcon Information Co., Ltd., Hangzhou, Zhejiang 310051, China*

[†]*Correspondence author Email: zhangwei@zstu.edu.cn*

ABSTRACT

The double-suction centrifugal fan is typically installed in the ventilation unit and driven by a motor beside it. One of the two inlets of the double-suction fan is partially blocked by the motor, and the flow in the fan becomes asymmetric and non-uniform. This work numerically investigated the effect of the motor blockage on the transient characteristics of the asymmetric flow in a centrifugal fan. The distance between the motor and the adjacent collector is typically 20mm or 40mm. Numerical results reveal that compared with the baseline motor-free model, the motor blockage of the two models decreases the flow rate by 30.4% and 20.8%, respectively, at the obstructed inlet of the fan, and the inflow is non-uniform and presents a local reversed flow. The motor blockage decreases the static pressure efficiency by 9.45% and 6.04%, respectively, while the static pressure rise is hardly affected. The flow fluctuation is notably asymmetric and non-uniform due to the non-axisymmetric geometry of the volute and the motor blockage. The blade passages are occupied by strong reversed flow, and a low-pressure region exists in the impeller. This work also performed a comparative study on the correctness and applicability of the boundary condition. The type of boundary condition of constant pressure at the outlet and a flow rate at the inlet, which is a common choice for fans without considering the obstacles, is analyzed. It was found that this type of boundary condition underestimates the efficiency of the fan with motor blockage, and the pressure field at the fan inlet is considerably different.

Article History

Received June 3, 2024
Revised August 22, 2024
Accepted November 3, 2024
Available online February 4, 2025

Keywords:

Double-suction
Centrifugal fan
Motor
Blockage
Asymmetric
Boundary condition

1. INTRODUCTION

The double-suction centrifugal fans are applied in the HVAC unit, considering their better compactness, lower noise, and accessible maintenance features. In practice, the fan is driven by a motor beside it; thus, one of the two inlets of the fan is partially blocked by the motor, and the inflow and internal flow are affected. The patterns of inflow are crucial for the aerodynamic, aero-acoustic, and vibration performance of the centrifugal fan (González et al., 2019; González et al., 2020; Wang et al., 2021) and other types of turbomachines (Chang et al., 2024; Li, 2024; Rong et al., 2024).

The geometrical and operational parameters determine the performance of the centrifugal fans. The design and optimization of the fan are customarily carried out by varying one or several parameters, especially the parameters of the rotating impeller for improved performance and reduced noise. The internal flow characteristics have been investigated in several works to reveal how single or multiple specific parameters affect. Zhao and Guan (2023) analyzed the influence of the impeller's spatial position within the centrifugal fan on its internal flow field. The variation of impeller's eccentricity angle, eccentricity, and longitudinal depth in the volute has different impact on the flow field. Zheng et al. (2023) investigated flow in the fan with different front disc geometry. They found that the curvature of the impeller front disc edge increases the through-flow area of the blade passage, and reduces the energy loss and improves the fan performance. Pathak et al. (2020) analyzed the internal flow of single-stage centrifugal blowers with different impeller configurations. The varied impeller geometry would indeed affect the flow inside the blower. Lun et al. (2019) numerically investigated the unsteady flow in a centrifugal fan at low flow rates. The vortices predominantly form near the volute outlet and volute tongue. Zhou et al. (2023) analyzed the noise generation

in the fan. The applicability of the bionic structures at the volute tongue, blade leading and trailing edges were evaluated. Chen et al. (2024) studied the specific configuration of inclined and offset impeller in a fan. The authors found that the impeller deviation results in significantly non-uniform flow, which degrades the fan performance (Chen et al., 2022).

The volute is designed to direct the air circulating in the fan and finally exits at the outlet. The aerodynamic compatibility between the volute and the impeller determines the fan's aerodynamic and aero-acoustic performances. Kim et al. (2013) optimized the impeller of a centrifugal fan. Nilugal et al. (2022) explored the benefits of a chamfered volute for the centrifugal ventilator; it was determined that a chamfer ratio of 4.4 results in superior performance characteristics, and this optimal configuration exhibits a static pressure rise improvement of approximately 6.3% compared to the baseline model. More et al. (2019) analyzed the effects of the impeller blade thickness and rotational speed and calculated the intrinsic frequency and total deformation for different blade thicknesses and speeds. The results indicated that a 1.5mm thickness blade exhibits lower noise and vibration at maximum speed. Tsurusaki and Kinoshita (2001) experimentally verified that the mainstream instability contributes to rotational stall. They demonstrated that the rotational stall can be reduced or amplified by the jet flow in the direction of θ=0° or 180°, respectively. Patil et al. (2018) investigated the performance variation of a centrifugal blower by adjusting the volute tongue clearance. Their findings indicated that the tongue clearance significantly influences the blower's performance parameters; as the tongue clearance decreases, the total pressure rise and efficiency increases. Hariharan and Govardhan (2019,2016) found that the parallel-wall volute enhances the performance of an industrial centrifugal blower. Kim et al. (2015) utilized a numerical simulation approach to visualize the flow with the air cleaner and predicted the noise.

The inflow affects the flow in the centrifugal fan. In practical applications, the fans often operate under specific inflow conditions, which are attributed to the environment in which the fan works. The geometry of the collector and the possible existence of external obstacles are typical influential factors. The influence of the inflow pattern was analyzed considering the significant modification of the fan's geometrical parameters. Liu et al. (2012) studied the influence of inlet geometry of a centrifugal fan; the area for the through-flow with significant meridional velocity near the blade tip was observed with a large collector. Li et al. (2023) explored the aerodynamic performance variation caused by the motor mounting height. The higher motor mounting results in lower static pressure rise and efficiency at large flow rates. Motohiko et al. (2003) conducted experimental research on the influence of the collector; the results revealed that as the size of the collector decreases, the meridional velocity decreases at the fan inlet and increases outside the blade tip. Qin et al. (2023) investigated the motor intrusion in a volute-free centrifugal fan; a significant reduction of performance quantities was observed at large flow rates. Lin and Chou (2004) analyzed the influence of the obstacles, which is quantified by the parameter of the distance between the fan and the flat obstacle. The obstruction had a more pronounced effect on the maximum pressure rise than the maximum flow rate. Li (2021) designed a collector and a non-uniform diffuser to match the low-speed, high-efficiency centrifugal impeller of the fan. The design regulates the pressure distribution in the impeller, increases flow rate, improves flow separation generated by the guide vanes, and enhances flow uniformity at the diffuser outlet. Sui et al. (2009) experimentally studied the outflow of an axial fan in the presence of the free outlet and flat impingement plate. Zhang and Vahdati (2019) explored the inflow distortion effect on the aerodynamic stability of fan blades, identifying parameters that primarily influence blade stability. Madhwesh et al. (2018) analyzed the effect of a circular front and rear fence of the centrifugal ventilator impeller; the size and location of the fence were optimized. Gunn et al. (2013) experimentally studied the internal flow of the fans under inflow distortion and found that the inflow distortion reduces the fan performance and stability. Kang et al. (2020) studied the model of an obstacle upstream of a fan; the obstacle increases the pressure loss and decreases the power coefficient, leading to performance degradation and unstable internal flow. MacDonald et al. (2009) considered the inlet clearance and inlet grille and studied the impact on flow and acoustic characteristics; the optimum inlet clearance is 2-3mm. Liu et al. (2022) analyzed the flow in a volute-free centrifugal fan; the fan inflow is generated by a curved pipe, and presents non-axisymmetric pre-swirl pattern at the fan's inlet. It was found that a curved section with a large radius stabilizes the flow, manifested by the relatively weak pressure fluctuation.

The works reviewed demonstrates the significance of geometrical parameters and inflow patterns on the performance of the fans. For the double-suction, multi-blade centrifugal fans employed in the ventilation or air conditioning circumstances, usually two or four fans are combined as a unit in which the neighboring two fans are driven by the same motor placed between them. In this condition, the motor partially blocks one of the two inlets of each fan, where the inflow patterns are affected. The motor blockage is considered in the experimental study, and the measured quantities represent the actual performance of the fan. However, in most numerical simulations, the fan performance is of interest, and the factors influencing the realistic applications are normally ignored, such as motor blockage and the limited space of the room where the fans are deployed. The predicted performance quantities and characteristics of internal flow in such a simplified model would produce less accurate data, which would be significant for manufacturers and users. The performance degradation by the motor blockage should be quantitatively evaluated to facilitate the fan's further design, optimization, and operation.

We numerically investigated the flow in a double-suction centrifugal fan to investigate the blockage effect of the motor placed on one side of the fan. Three models were setup, including the baseline motor-free model and two models with the motor placed at a distance of 20mm and 40mm away from the nearby collector, respectively.

We focused on the motor blockage effect of the transient characteristics of asymmetric flow in the fan. The inflow patterns in both collectors are comparably explored in terms of pressure and velocity fields to reflect the flow's non-uniformity. The transient flow separation and pressure and velocity fluctuation in the impeller and volute were also studied.

The correctness and applicability of the boundary condition of the simulations were also analyzed in this work. The type of boundary condition of constant static pressure at the fan outlet and constant flow rate at the fan inlet, a common choice for the fan model in a lot of numerical investigations, was employed in a separate simulation, and the results are compared with the present simulation. The comparative assessment aims to reveal the inaccuracy of the inappropriate type of boundary condition, which should be avoided in further simulations.

2. NUMERICAL DETAILS

2.1 Physical Model

Fig. **1** presents the baseline model of the double-suction centrifugal fan. The fan comprises the volute, impeller, and two collectors as the main components and the bearing bracket and pedestal as accessories. The air moving through the collector is driven by the rotating impeller, circulates and finally moves out of the volute outlet. The operational and geometrical parameters are listed in Table 1.

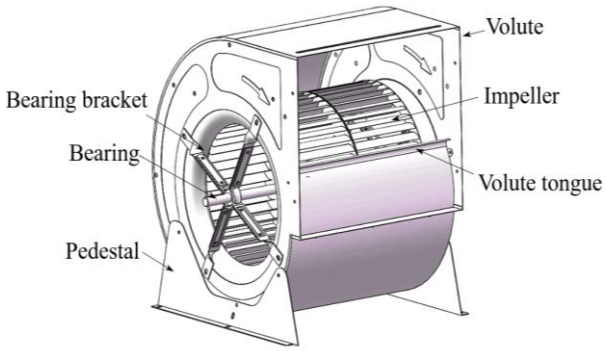

Fig. 1 Double-suction centrifugal fan

Table 1 Geometric and operational parameters

Parameter	Value
Rotational speed	600rpm
Designed flow rate	7488m^3/h
Impeller radius at inlet	191mm
Impeller radius at outlet	231mm
Blade angle at inlet	95.63°
Blade angle at outlet	171.78°
Blade number	48
Impeller width	440mm
Volute height	736.44mm
Volute width	552mm
Volute outlet width	301.91mm
Volute tongue radius	15mm

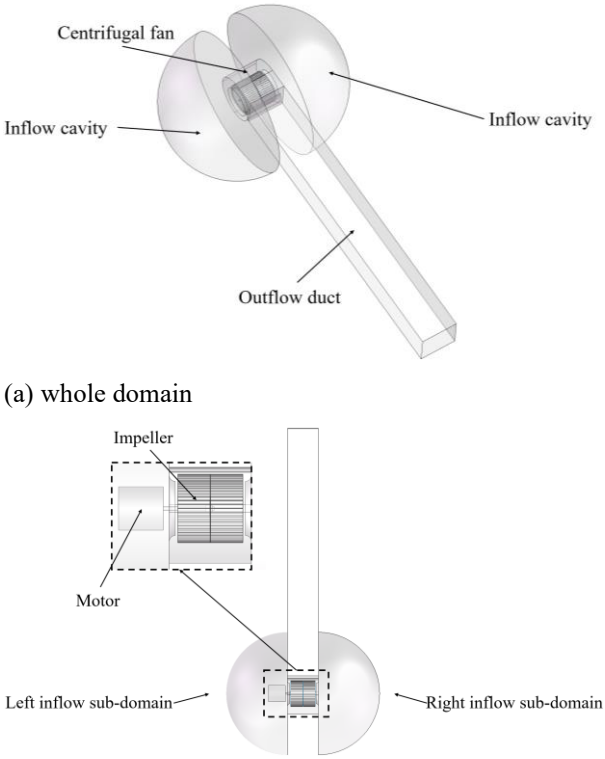

(a) whole domain

(b) side view and the motor

(c) separating distance is defined as L

Fig. 2 Computational domain

The computational domain for the numerical simulation is given in Fig. 2a. It consists of the fan, the two inflow cavities to both sides of the fan to represent the open room, and the outflow duct, which permits the air to exit from the fan. The model considers the central shaft, while the bearing brackets are ignored since they are small and twisted to impose negligible blockage on the inflow. The selection of the computational domain size is crucial. A small domain may result in significant boundary effects, impacting the accuracy of the simulation results. Conversely, an excessively large domain would waste the computational resources. In this work, the radius of the inflow cavity is six times the collector's diameter, and the length of the outflow duct is eight times the impeller outlet's diameter, which we believe are sufficient for the simulation based on our experience (Liu et al., 2022; Chen et al., 2024).

The motor driving the impeller is placed in the left

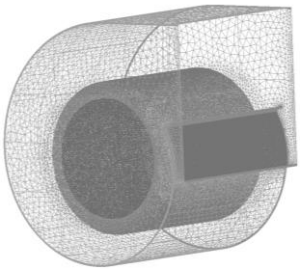

(a) centrifugal fan

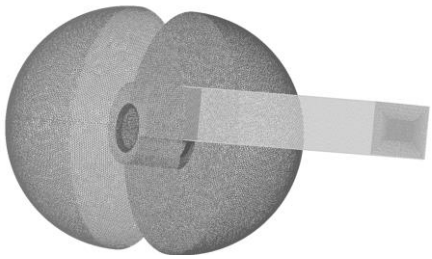

(b) whole domain

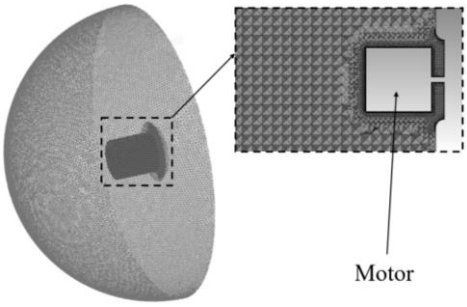

(c) left inflow sub-domain with the motor

Fig. 3 Grid layout

inflow sub-domain, as seen in Fig. 2b. The motor is simplified as a cylinder whose diameter and length are 292mm and 300mm, respectively. The distance between the surface of the motor and the adjacent collector is labeled as L, as seen in Fig. 2c. In this work, we set up two models with L=20mm and 40mm, denoted as Model-20mm and Model-40mm, respectively, and the baseline motor-free model used for comparison is denoted as Model-BM in the following discussions.

2.2 Numerical Methods

The numerical simulations were conducted using ANSYS-Fluent. The 2nd-order upwind and central difference schemes were used to discretize the convective and viscous terms, respectively. The pressure and velocity were coupled using the SIMPLE method. The outlet flow rate is constant, and the inlet static pressure is zero; no-slip velocity applies for walls.

We first performed a RANS simulation with a convergence residual 10^{-3} to obtain the guess solution rapidly. The converged solution was then used as the initial solution for the transient large-eddy simulation (LES). The time step was 2.778×10^{-4} seconds, i.e., the impeller rotating for one degree. The LES was first conducted for ten impeller revolutions, then for three revolutions to obtain the time-averaged quantities, and finally for one impeller revolution for data acquisition and statistics.

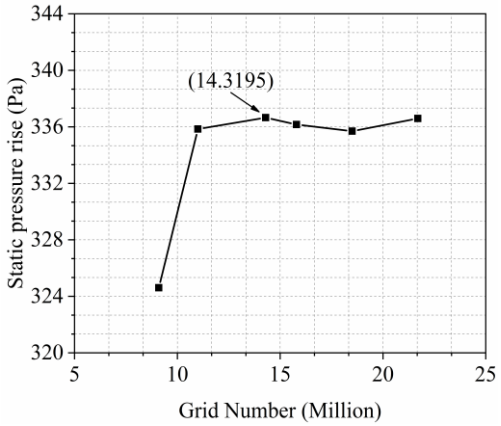

Fig. 4 Variation of static pressure rise with grid number

Table 2 The grid details

Domain	No. grids (in thousands)
Impeller	10499
Volute	1229
Inflow cavity	1068
Outflow duct	1523
Total	14319

2.3 Grid Independence Study and Validation

The hybrid structured-unstructured grid is generated using the software ANSYS ICEM-CFD. The structured grid discretized the impeller and outflow duct, while the sub-domains of the volute and inflow cavity were discretized using the unstructured grid, as seen in Fig. 3. The grid was refined on all walls with eight layers of cells of constant size; the first-layer grid has a size of 0.3mm, corresponding to a maximum value of y^+ around 2.

To ensure the grid resolution's sufficiency for the accurate flow physics prediction, the grid sensitivity study was performed for Model-BM at the designed flow rate using the RANS simulation with SST k-ω turbulence model. Six grids were generated, with the number of cells approximately 9.1, 11.0, 14.3, 15.8, 18.5 and 21.7 million. Fig. 4 shows the static pressure rise obtained using various grids. The static pressure rise reaches 336.6Pa for the grid with 14.3 million cells, and the further increasing of the grid number produces a negligible impact. Therefore, the grid with 14.3 million cells is suitable for the simulations, enabling it to effectively capture the flow field characteristics, including the boundary layer flow and turbulent structures. It is reasonable to infer that the grid is also suitable for the LES simulations. The grid details are listed in Table 2. For the models with the motor, i.e., Model-20mm and Model-40mm, the grid is slightly varied since the motor was considered, while the total number of cells was roughly the same as that of Model-BM. The modification of the grid was conducted in the left inflow cavity.

In the validation, the numerical simulations were performed for Model-BM using the grid with 14.3 million cells. Fig. 5 gives the fan performance quantities, and are compared with the experimental data. The numerical

Table 3 Aerodynamic quantities of various models

Model	Model-BM		Model-20mm		Model-40mm	
	Left	Right	Left	Right	Left	Right
Volume flow rate (m^3/h)	3685	3803	2565	4923	2919	4569
Static pressure rise (Pa)	335.98	340.84	340.28	345.51	347.35	346.14
Static pressure efficiency (%)	64.12		54.67		58.08	
Power (kW)	1.011		1.080		1.061	

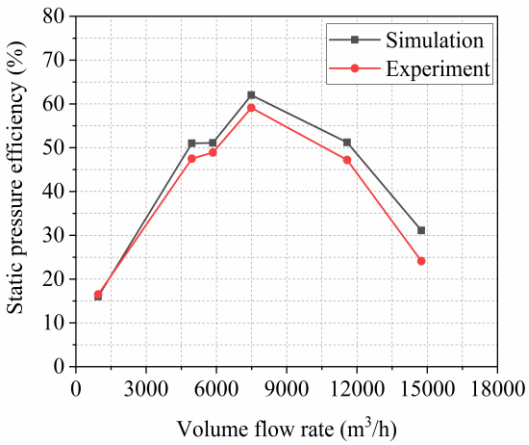

(a) static pressure efficiency

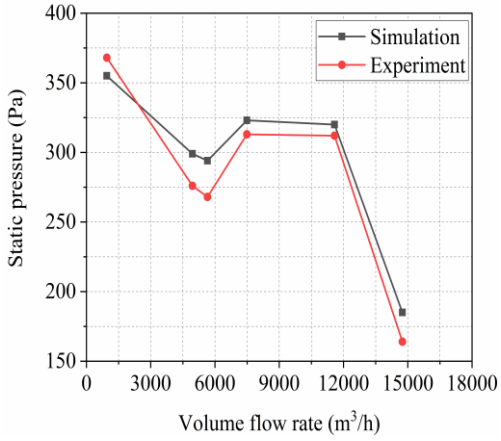

(b) static pressure rise

Fig. 5 Validation of numerical data

data is generally consistent with the experimental data at all flow rates, although its magnitude is slightly higher due to the neglect of the leakage and loss. At the designed flow rate of 7488m³/h, the two quantities are 3.2% and 4.5% higher than the experimental data, and the relative difference is 9.7% and 4.3% in the volume flow rate of 5650m³/h. Therefore, we believe the numerical simulation is reliable in revealing the essential flow physics.

3. RESULTS AND DISCUSSION

3.1 Fan Performance

The motor blockage of one inlet of the fan results in asymmetric flow at the fan's inlet. The volume flow rate at the two inlets, representing the amount of air entering the fan, is unequal, and the static pressure rise is also different. Table 3 lists the time-averaged volume flow rate and static pressure rise at the two inlets, and the fan's static pressure efficiency and power of the three models. The time-averaging was performed for a duration of three impeller revolutions. The flow rate of the two inlets of Model-BM is roughly the same; the minor difference is mainly attributed to the simulation's limited averaging duration and the flow's inherent asymmetric feature.

For the two models with the motor, it is seen that the motor blockage on the left inlet of the fan reduces the flow rate by 30.4% and 20.8%, respectively; the reduction of flow rate is more remarkable for Model-20mm since the motor is placed closer to the fan. However, different from the observation of flow rate, the static pressure rise is relatively close for all three models, and the magnitude is slightly higher for the models with motor, although the difference is minor. It is due to the accelerated inflow as the air deviates from its direction as the motor obstructs it. Compared with Model-BM, the motor blockage notably decreases the efficiency by 9.45% and 6.04% for Model-20mm and Model-40mm, respectively. Since the static pressure rise is almost unaffected, the deteriorated efficiency is due to the increased torque, which is also reflected by the increased power of the fan.

The temporal variation of surface-averaged static pressure is presented in Fig. 6 for five impeller revolutions. For Model-BM, the static pressure weakly fluctuates around the mean value, and the fluctuation of the two inlets are generally the same. The introduction of the motor significantly intensifies the pressure fluctuation. The fluctuation gets stronger for both inlets of Model-20mm and Model-40mm and is quasi-synchronous; the fluctuation is more substantial for Model-20mm as the inflow obstruction is strong. It is also observed from the figure that the low-frequency fluctuation dominates rather than the high-frequency fluctuation for Model-BM.

3.2 Asymmetric Inflow in the Collector

The motor blockage first alters the patterns of flow in the collectors. Fig. **7** presents the instantaneous streamlines distribution in the inflow cavities and the fan. The streamlines for Model-BM are symmetric on the two sides of the fan and exhibit a uniform inflow at the collector. The flow transitions direction from axial to radial, which is evident as the curved streamlines with high velocity magnitude. As the left inlet of the fan is blocked by the motor, the flow becomes non-uniform. The air enters the fan primarily through the gap between the motor and the collector, generating disordered fluid motion in the central region of the fan inlet. This irregularity is particularly noticeable for Model-20mm with a smaller gap. The inflow from the right inlet of the fan is accelerated to maintain the constant volume flow

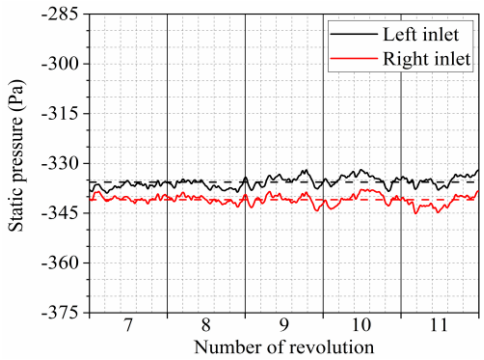

(a) Model-BM

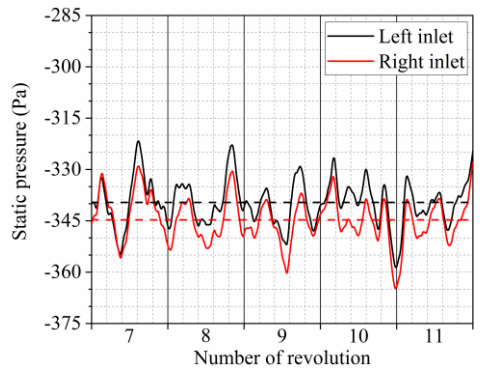

(b) Model-20mm

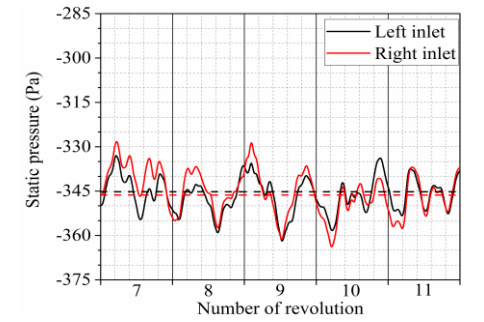

(c) Model-40mm

Fig. 6 Time history of the static pressure at both fan inlets

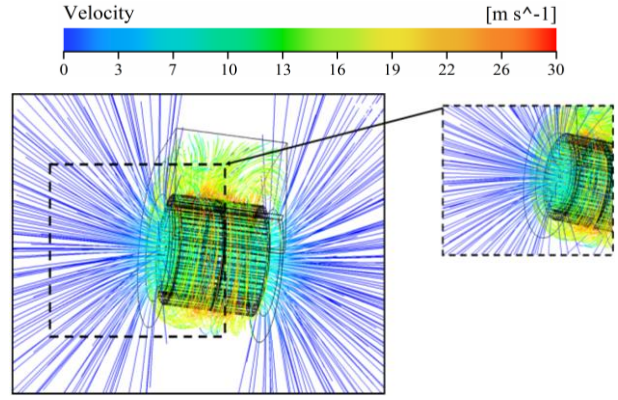

(a) Model-BM

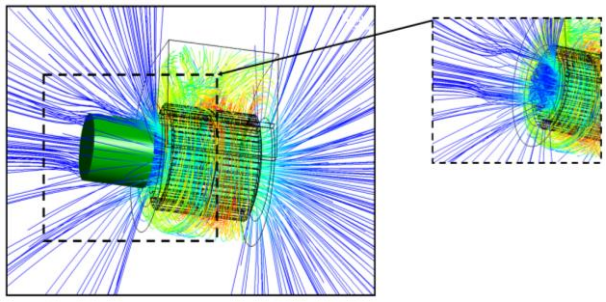

(b) Model-20mm

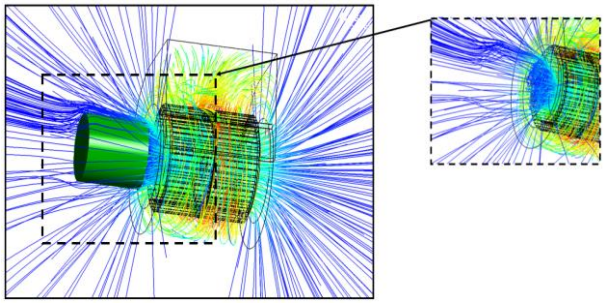

(c) Model-40mm

Fig. 7 Instantaneous streamlines colored by the magnitude of velocity

rate, and the motor does not affect the local flow patterns.

Fig. 8 shows the static pressure field at the collector's inlet. For Model-BM and the right collector of Model-20mm and Model-40mm, where the inflow is not affected by any obstacle, the static pressure is high in the central cross-section but gets reduced to the boundary. The motor primarily decreases the pressure in the central cross-section. As observed for Model-BM, the high-pressure region is almost eliminated for the left inlet of the Model-20mm fan, and the low-pressure region close to the boundary also slightly expands. For Model-40mm, since the motor is placed away from the collector, the pressure in the central region of the right cross-section is comparably higher than that of Model-20mm. For the right collector, since the local flow is accelerated especially in the boundary region of the collector, as seen in Fig. 7, the static pressure is lowered compared with the baseline model, and the magnitude is also weakly decreased in the central region.

Since the motor partially blocks the left collector's inlet, the air has to move in the radial direction before it enters the collector. The characteristics of the velocity field are used as an indicator of the influence of motor blockage. Fig. 9 shows the instantaneous radial velocity field at the collector's inlet. It is defined positive as the air moves toward the collector's center. The radial velocity at the left inlet is noticeably affected by the motor but is almost unaffected at the right inlet in terms of magnitude and direction. For the Model-20mm and Model-40mm fans, the velocity is positive primarily in the left and bottom regions, reflecting that the local fluid moves toward the center after it across the motor. It is especially notable for the Model-40mm fan, where the motor is placed away from the collector; we believe it is attributed to the larger space that permits the complete velocity

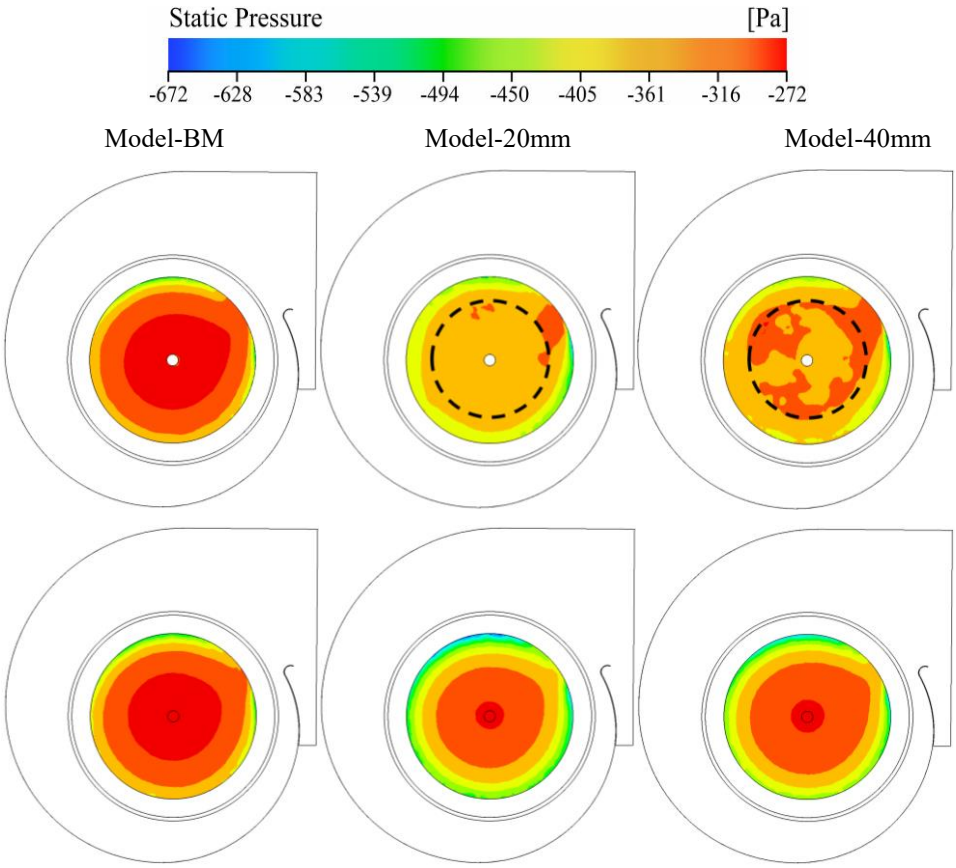

Fig. 8 Instantaneous static pressure field at the collector's inlet. The top sub-figures for the left inlet; the bottom sub-figures for the right inlet. The dashed line represents the position of the motor

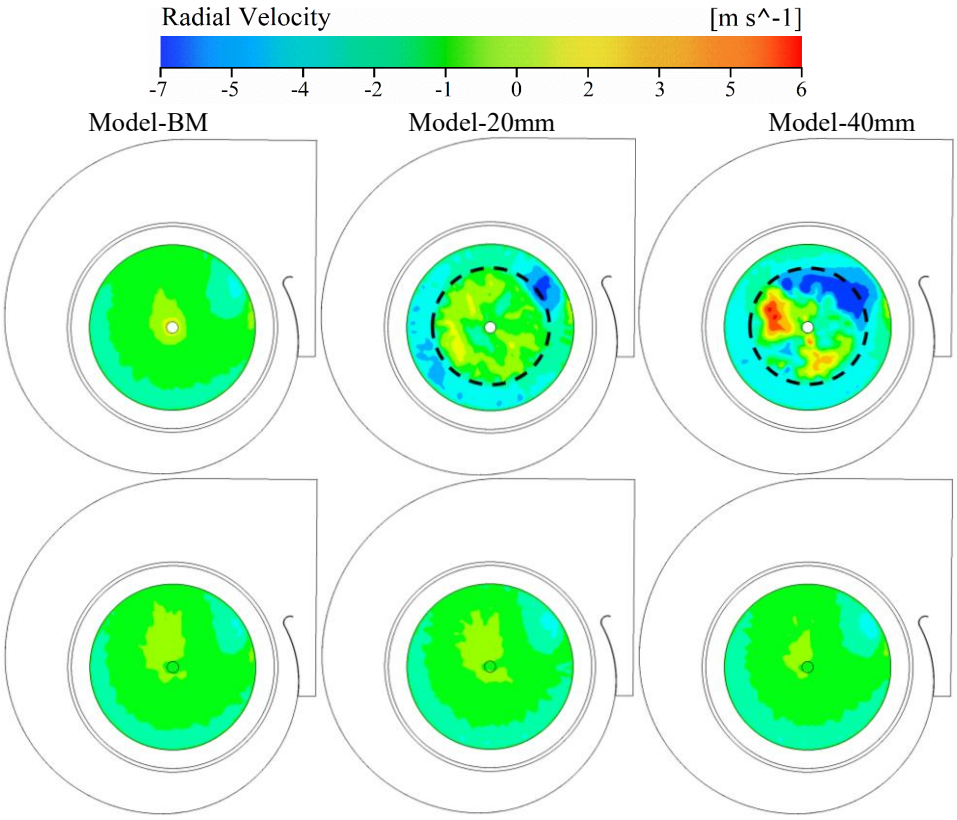

Fig. 9 Instantaneous radial velocity field at the collector's inlet. The top sub-figures for the left inlet; the bottom sub-figures for the right inlet. The positive value of the radial velocity represents the fluid moving toward the center of the collector. The dashed line denotes the position of the motor

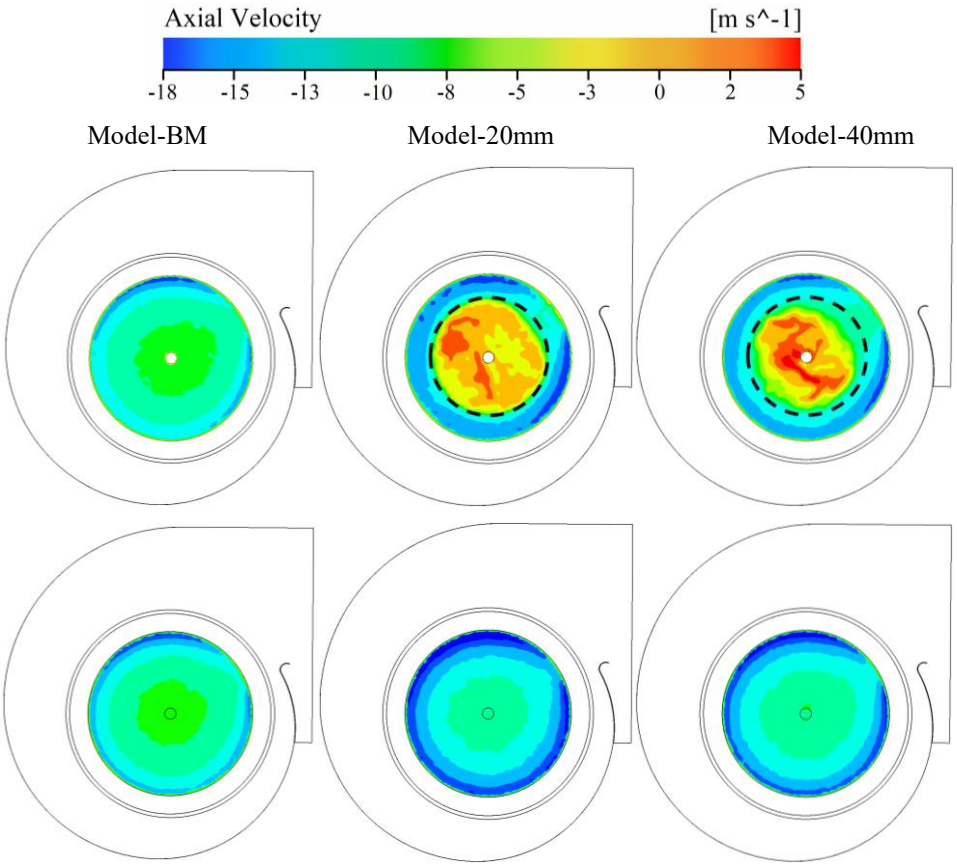

Fig. 10 Instantaneous axial velocity field at the collector's inlet. The top sub-figures for the left inlet; the bottom sub-figures for the right inlet. The negative value of the axial velocity denotes the flow moving toward the interior of the fan. The dashed line represents the position of the motor

direction transition. There is fluid with negative radial velocity close to the volute tongue, observed in both Model-20mm and Model-40mm. The non-uniform radial velocity results from the rotating impeller, which guides the flow toward the fan outlet.

The motor blockage also affects the collector's through-flow capability. The instantaneous axial velocity field at the collector's inlet is shown in Fig. 10; the negative value of axial velocity represents flow toward the interior of the fan, i.e., forward flow. As the inflow is unaffected by the motor, the axial velocity exhibits a distribution like concentric circles; the magnitude is relatively smaller in the central cross-section, while it is more significant at the boundary, especially for the right inlet of Model-20mm and Model-40mm due to acceleration as the fluid moves on the curved section of the collector. For the left inlet of Model-20mm and Model-40mm with motor blockage, the velocity magnitude in the central cross-section greatly reduces. The decreasing is more substantial for Model-20mm. It is noted that reversed flow with positive axial velocity emerges locally, although with a small magnitude, due to the highly perturbed inflow by the motor. The reversed flow occupies 25.8% and 19.5% of inlet area for Model-20mm and Model-40mm, respectively. The magnitude is small in the top-right region, i.e., close to volute tongue, for both Model-20mm and Model-40mm, which is also observed in Fig. 9 as the rotating impeller drives the air to move directly toward the fan outlet.

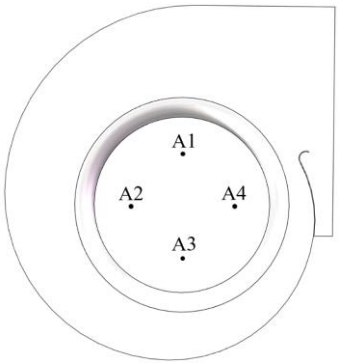

Fig. 11 Position of the monitors at the collector's inlet

The field of the static pressure, radial velocity, and axial velocity at the collector inlet reveal that the motor deteriorates the circumferential uniformity of the through-flow by decreasing the axial velocity in the majority area of the cross-section, and the distribution is circumferentially non-uniform. The rotating impeller drives the air toward the volute tongue, producing remarkable non-uniform flow. To further analyze the circumferentially non-uniform flow in the collector, four monitors are evenly set over the circumference of the collector with a distance to the center as half the radius of the inflow cross-section and are labeled as A1/A2/A3/A4, as seen in Fig. 11. The monitors are set in both the left and

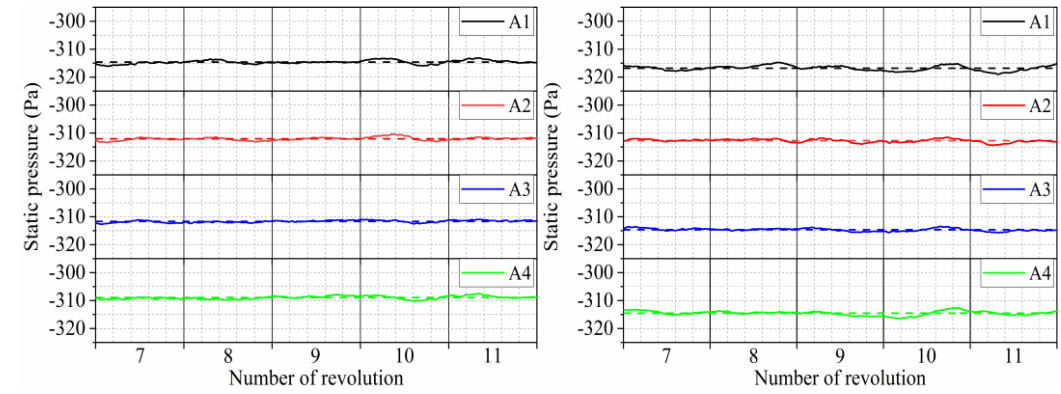

(a) Model-BM

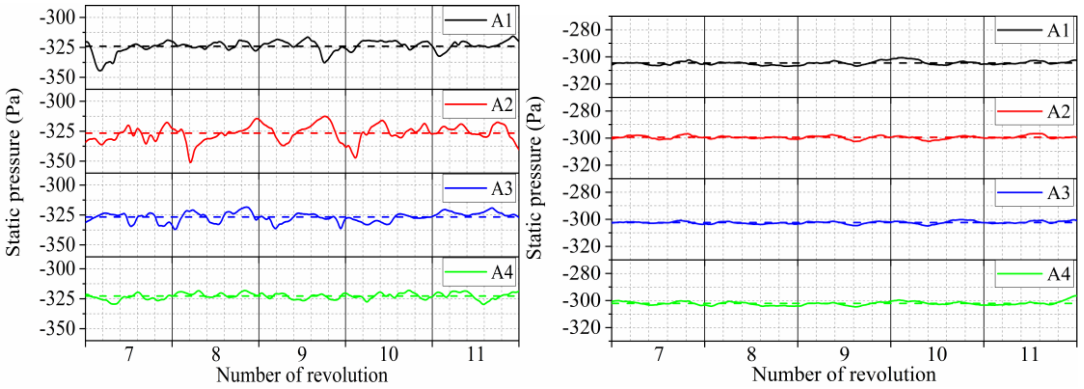

(b) Model-20mm

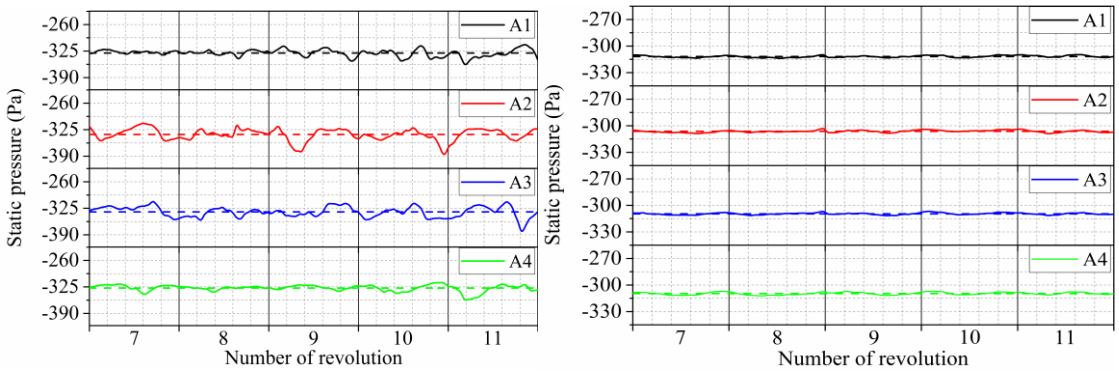

(c) Model-40mm

Fig. 12 Time history of the static pressure. The left sub-figures for the left collector; the right sub-figures for the right collector

right collectors. Fig. **12** shows the time history of static pressure. The pressure fluctuation is minor on both inlets of Model-BM; however, it becomes stronger in amplitude with low-frequency modulation for the left inlet of the Model-20mm and Model-40mm fans. The fluctuating amplitude is the most noticeable for monitor-A1, -A2, and -A3, which are located far from the volute tongue, and is relatively minor for monitor-A4 as the volute tongue restricts the flow.

The fluctuation of the static pressure is quantified by its mean and root-mean-square (RMS) fluctuating component as listed in Table 4 and

Table **5**. The two quantities are defined as:

$$p_{\text{avg}} = \frac{1}{\Delta t}\int_{t_0}^{t_1} p dt \tag{1}$$

$$p'_{\text{rms}} = \sqrt{\frac{\int_{t_0}^{t_1}\left(p - p_{\text{avg}}\right)^2}{\Delta t}} \tag{2}$$

The time-averaged pressure obtained by the various monitors on the same collector is close in magnitude; the magnitude is generally in proximity for Model-BM and is lower for the left collector for Model-20mm and Model-40mm as a result of the motor blockage. The difference of p'_{rms} is much more pronounced for Model-20mm and Model-40mm than Model-BM, and it is especially notable for the former, in which the motor destabilizes the flow. The static pressure fluctuation is most pronounced at monitor-A2 and is notable for monitor-A1 and -A3, in which the motor perturbs the air entering the collector. However, the inflow close to the volute tongue is also

Table 4 Time-averaged static pressure

Monitor	Model-BM		Model-20mm		Model-40mm	
	Left	Right	Left	Right	Left	Right
A1	-314.63	-316.83	-324.11	-304.59	-329.76	-311.91
A2	-312.11	-312.77	-326.67	-299.46	-336.68	-306.41
A3	-311.69	-314.68	-326.78	-302.44	-333.94	-309.63
A4	-308.95	-314.53	-322.79	-302.17	-327.89	-309.64

Table 5 RMS value of the fluctuating static pressure

Monitor	Model-BM		Model-20mm		Model-40mm	
	Left	Right	Left	Right	Left	Right
A1	0.68	0.94	26.35	2.02	8.60	1.13
A2	0.59	0.60	47.60	1.15	14.41	1.24
A3	0.42	0.54	16.24	0.98	13.11	1.09
A4	0.59	0.81	6.90	1.95	7.99	1.45

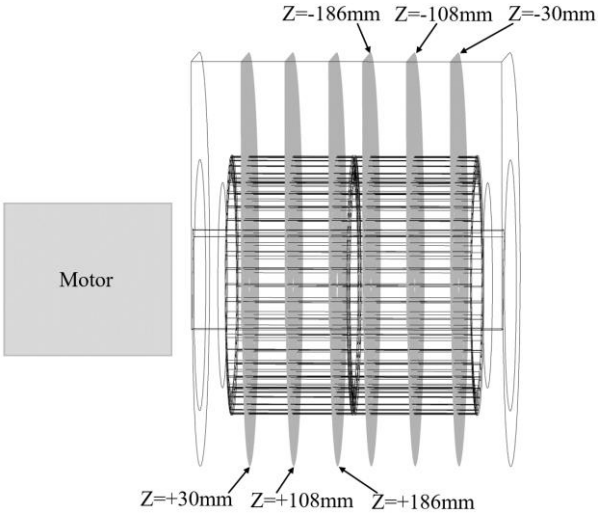

Fig. 13 Definition of the axial cross-sections

greatly affected by the rotating impeller and the fan's outflow; it is more regularized and presents a lower value of p'_{rms}.

3.3 Flow in the Impeller: General Characteristics

The flow characteristics are analyzed to reveal the influence of motor blockage on flow in the impeller. To demonstrate the asymmetric characteristics of flow on the two sides of the fan, the numerical data are presented on six cross-sections, as shown in Fig. 13. The cross-sections at Z=+30mm, +108mm, and +186mm are on the left half fan whose inlet is blocked by the motor, and they are located near the inlet, in the middle and near the central disc of the impeller, respectively. Similarly, the cross-sections at Z=-30mm, -108mm, and -186mm are on the right half fan, where the inflow is unaffected.

Fig 14 presents the instantaneous static pressure field for Model-BM. The magnitude gradually grows from the impeller to the volute. It is the maximum at the volute tongue and outer surface of the baffle. The static pressure in the blade passages is comparably low as the impeller rotation accelerates the air. The pressure distribution is almost the same for the six cross-sections since the inflow is not affected.

The instantaneous static pressure field for Model-20mm and Model-40mm is shown in Fig. 15 and Fig. 16, respectively. It is seen that, unlike in Model-BM, the pressure is notably low in the blade passages on the Z=+30mm and Z=+108mm cross-sections for the models with motor blockage. For the Model-20mm fan, the low-pressure region occupies almost the whole impeller except for several blade passages near the volute tongue, and it is the most pronounced near the top of the fan. The low-pressure region is indistinguishable at Z=+186mm; the magnitude is slightly lower than that of Model-BM but is only observable at the blade passage inlet. It reduces in size and the magnitude of negative pressure for the Model-40mm fan; it is notable in the several blade passages on the Z=+30mm cross-section upstream and downstream of the volute tongue, and is inconspicuous for the Z=+108mm and Z=+186mm cross-sections. The instantaneous static pressure in the right half fan is also affected by the motor blockage due to the increased flow rate, which alters the incidence angle as the flow transitions from axial to radial as moving through the blade passages. Similar to flow in the left half fan, the low-pressure region is the most pronounced in a portion of blade passages upstream and downstream of the volute tongue for the Z=-30mm and Z=-108mm cross-sections. Moreover, the pressure at the fan outlet is reduced in both sides of the fan, especially for Model-20mm.

Since the flow in the left half fan is affected by the motor blockage, the distribution of the instantaneous streamlines is presented in the Z=+30mm, Z=+108mm, and Z=+186mm cross-sections in Fig. 17. The streamlines are colored by the magnitude of velocity, which reflects the acceleration or deceleration of the local flow. The circulating flow in the blade passages of Model-BM exhibits minor separation; the separation is mainly observed at Z=+30mm where the inflow transits to radial direction. The circulating flow at Z=+108mm and Z=+186mm reduce in size and are mainly observed near the volute tongue, which prohibits the passage flow development. The motor perturbs the flow entering the fan

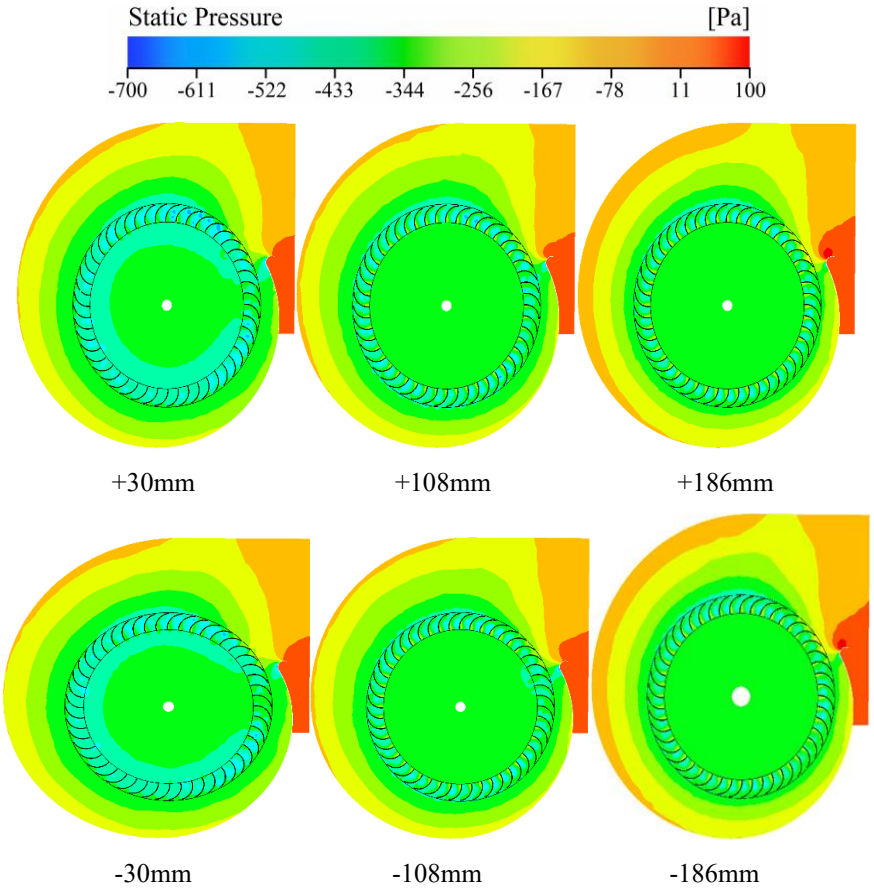

Fig 14 Instantaneous static pressure field for Model-BM

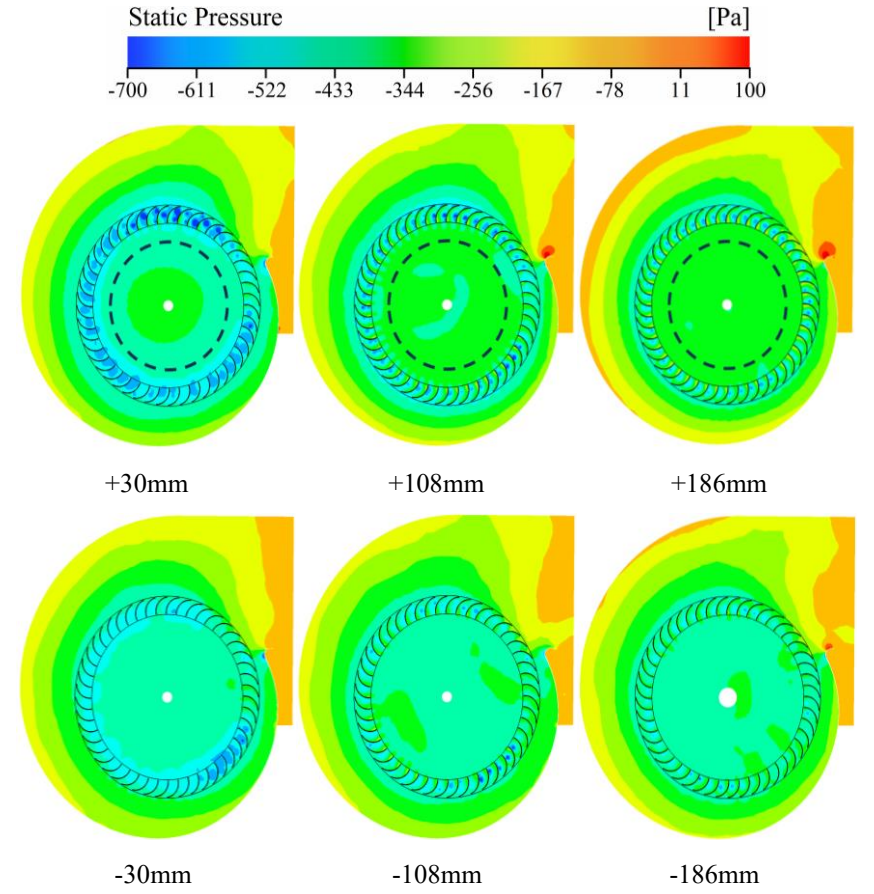

Fig. 15 Instantaneous static pressure field for Model-20mm

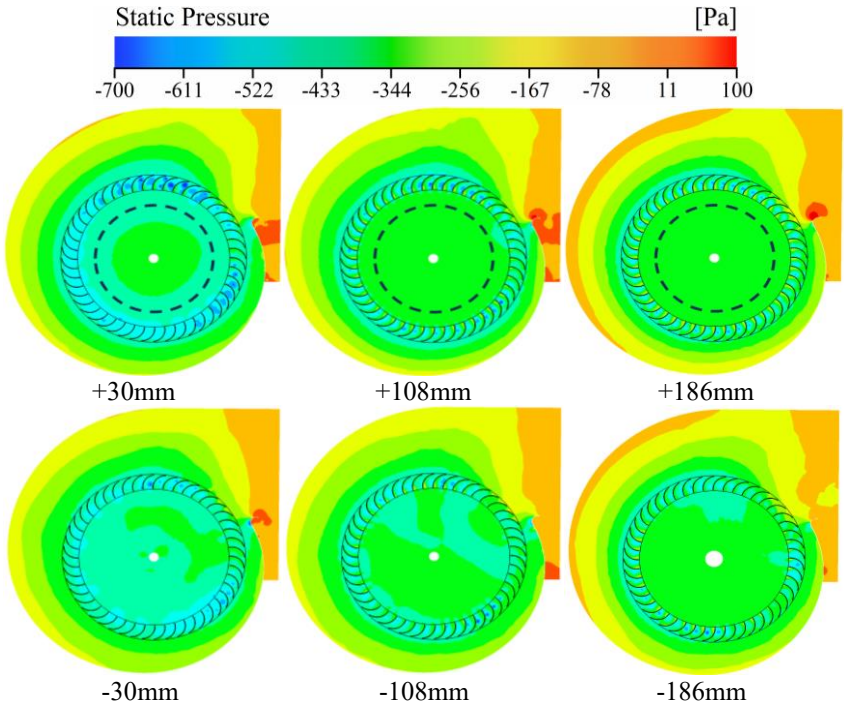

Fig. 16 Instantaneous static pressure field for Model-40mm

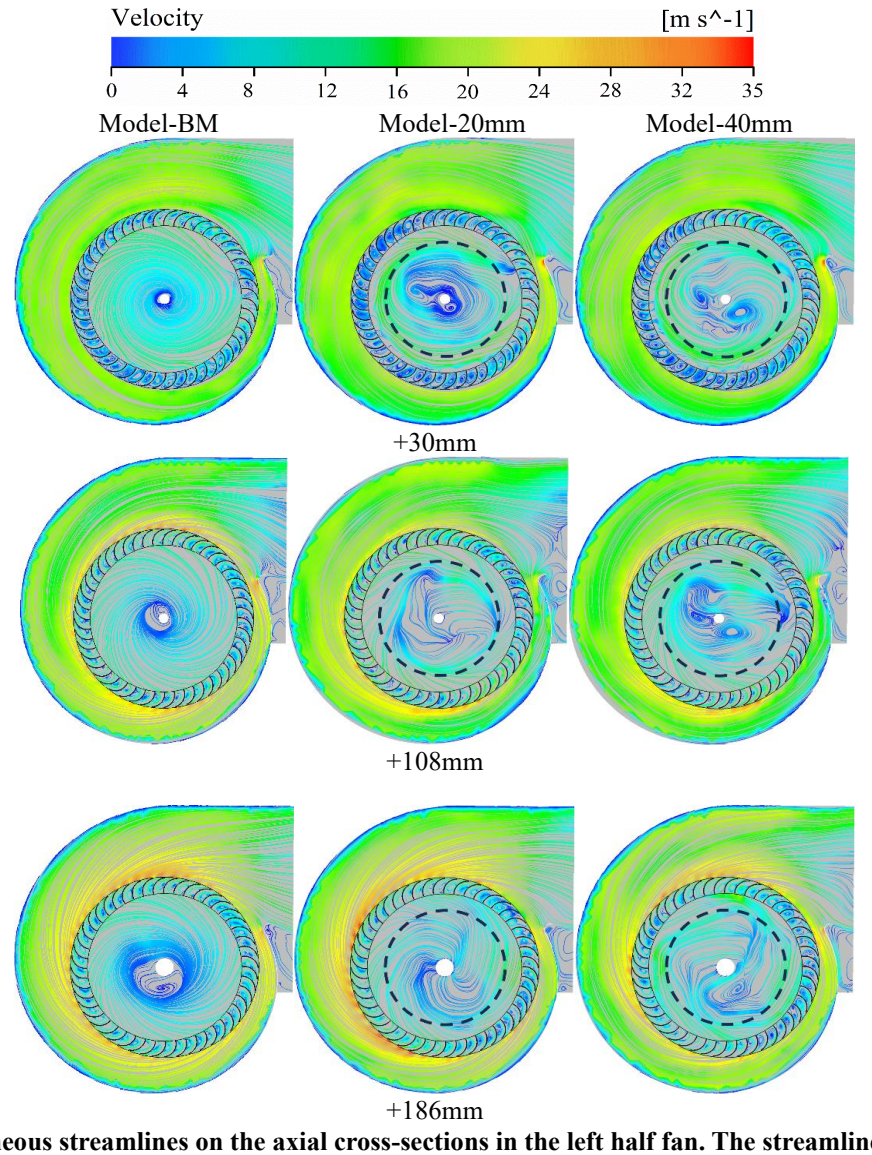

Fig. 17 Instantaneous streamlines on the axial cross-sections in the left half fan. The streamlines are colored by the magnitude of velocity

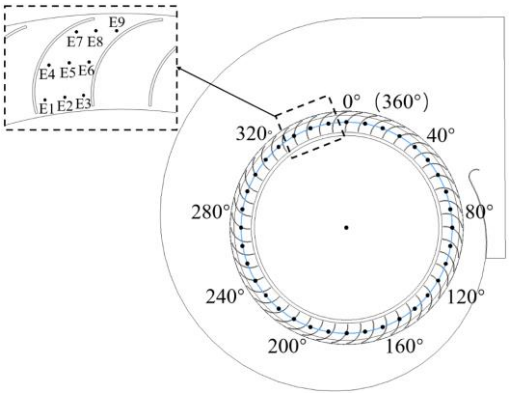

Fig. 18 Position of monitors

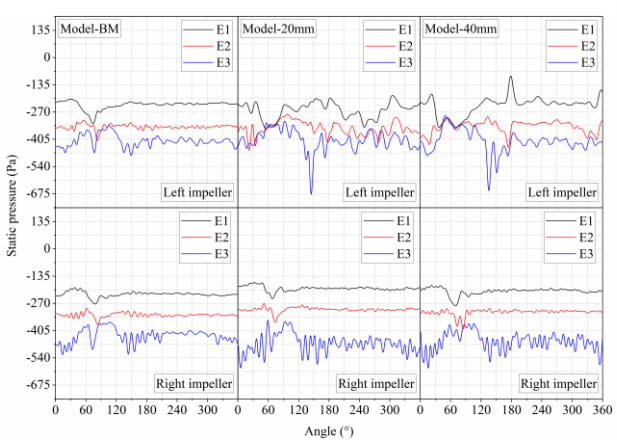

(a) monitor-E1/E2/E3

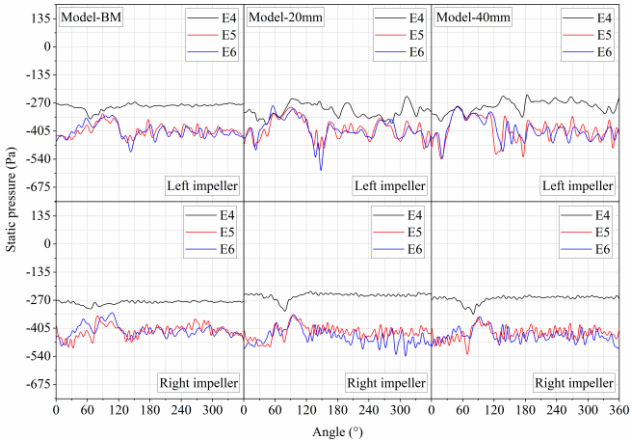

(b) monitor- E4/E5/E6

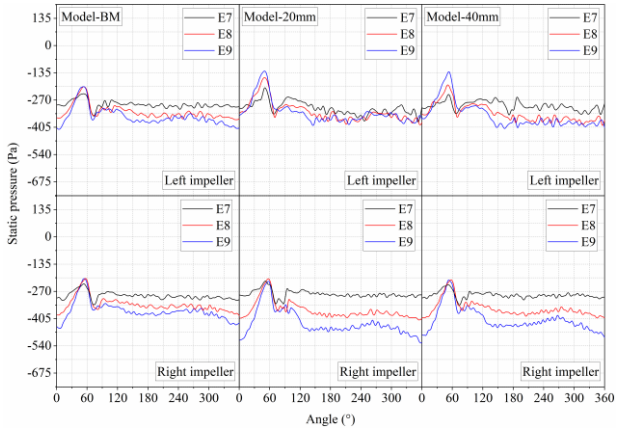

(c) monitor-E7/E8/E9

Fig. 19 Time history of static pressure for one impeller revolution

and results in the non-axisymmetric flow in the central impeller; the local flow is circumferentially non-uniform and alters the patterns of flow entering the blade passages. It is seen that for the Model-20mm fan, separated flow is formed in all blade passages at Z=+30mm; the circulating flow reduces in size in the blade passages away from the volute tongue at Z=+108mm and Z=+186mm. The circulating flow of the Model-40mm fan is further reduced in size and occupies less blade passages, reflecting the less significant motor influence.

In addition to the general characteristics of the flow presented in an instantaneous manner, we further analyze the transient flow as the impeller rotates for one revolution. A few monitors are set in one blade passage at Z=±108mm, as shown in Fig. 18. The monitors E1/E2/E3, E4/E5/E6, and E7/E8/E9 are set in the blade passage's inlet, middle, and outlet regions, respectively. The circumferential coordinate is represented by the angle. The static pressure and radial velocity are recorded on these monitors.

The transient behavior of static pressure is presented in Fig. 19. The fluctuating behavior depends on the monitor's position on either side of the fan and its position

within the blade passage. Some characteristic variations are generally applied for all monitors. The magnitude is roughly the smallest on monitor-E1/E4/E7 near the pressure surface, and largest on monitor-E3/E6/E9 near the suction surface. The static pressure fluctuates more significantly for monitors in the left impeller but is relatively weak for those in the right impeller, and the fluctuation near the suction surface is always the strongest, i.e., monitor-E3/E6/E9, attributed to the formation of evolving circulating flow due to flow separation.

For the Model-BM fan without the motor blockage, the transient fluctuation is quite similar in trend in the two halves of the fan, although not identical, considering the persistent occurrence of complex rotor-stator interaction and turbulent fluctuation. For monitor-E1/E2/E3, the magnitude decreases from monitor-E1 to monitor-E3. It is interesting to notice that there is a drastic decreasing of static pressure in the region 60°-90° for all monitors in both halves, with a rapid recovery in which the magnitude approaches a constant value. We can see from Fig. 18 that the decrease and recovery occur as the blade passage passes over the volute tongue; thus, the drastic variation results from the rotor-stator interaction. The phenomenon is not observed for monitor-E4/E5/E6. Although there are pronounced variations, especially for monitor-E5/E6, the fluctuation in the two sides is asynchronous due to the evolution of circulating flow. The transient characteristics of static pressure at the blade passage outlet, i.e., on monitor-E7/E8/E9, are pretty close in magnitude compared with other groups of monitors. The static pressure reaches the maximum for monitor-E7/E8/E9 almost right at the circumferential position of 60°; considering that these monitors are located at the impeller outlet, the local flow is the strongest perturbed by the volute tongue, but the variation tendency is contrary with monitor-E1/E2/E3 at the blade passage inlet.

The motor perturbs the static pressure in the left impeller but has a minor impact for the right impeller. The fluctuation is significantly amplified for monitor-E1/E2/E3. The static pressure at circumferential position of 60° does not present the drastic decreasing as for Model-BM; however, it increases for monitor-E2/E3 for the Model-20mm and Model-40mm fans, reflecting that the motor imposes different influence on the flow in different region of the blade passage. The static pressure at monitor-E3 exhibits a jump at around 150° for both models, consistent with the observation in Fig. 15-Fig. 17 that the noticeable local low-pressure region forms due to flow separation. It is also observed for monitor-E5/E6 located in the middle blade passage; it is evident for Model-20mm but inconspicuous for the Model-40mm fan. The influence of motor blockage is less significant for the flow near the blade passage outlet; the transient fluctuation is quite close for the three models.

3.4 Flow in the Impeller: Transient Characteristics

For the centrifugal fan with forward-curved blades, the forward through-flow moves generally along the radial direction with circumferential motion due to the curved blade. The radial velocity could indicate the through-flow capability of the blade passages, and its direction denotes the forward or reversed flow. The transient characteristics of the radial velocity are shown in Fig. 20. The negative radial velocity represents the reversed flow in the blade passage. For Model-BM, the reversed flow due to local boundary layer flow separation is observed for monitor-E3 and monitor-E6, which are located adjacent to the suction surface; the local reversed flow is almost persistent for the whole impeller revolution and occurs in both sides. The radial velocity at monitor-E9 is positive, indicating that the local flow becomes a persistent forward flow. The radial velocity at other monitors is always or primarily positive; the flow adjacent to the pressure surface is quite stable, with minor fluctuation during the impeller revolution. The magnitude experiences a drastic decreasing at 60°-90°, which is noticeable for monitor-E2/E5/E8, due to the volute tongue confinement which obstacles the impeller outflow; thus, the pressure gradient decelerates the passage flow.

Compared with Model-BM, the introduction of the motor results in a more significant fluctuation of radial velocity and more intense reversed flow, especially for flow in the left impeller. The fluctuating amplitude is more significant for Model-20mm and the monitors close to blade surfaces. The influence from motor blockage is the most significant for flow at the blade passage inlet, as observed from the curves for monitor-E1/E2/E3. It is seen that the intensified fluctuation is remarkable as the blade passage moves around the volute tongue. The flow is then stabilized, suggested by the less fluctuating radial velocity, as the blade passage moves away. The phenomenon is more evident for Model-40mm, where the motor blockage is weaker than that for Model-20mm. It is also shown that the decreasing radial velocity at the circumferential position around the volute tongue is pronounced for all monitors.

The impact of motor blockage on flow at monitor-E4/E5/E6 is not as strong as for flow at the inlet. However, the radial velocity presents an intensification; the fluctuating amplitude for monitor-E5 in the central passage is the largest. The influence of motor blockage on flow near the blade passage outlet is even weaker. The radial velocity of the flow in the central passage is shortly negative as the blade passage approaches the volute tongue. As the impeller further rotates, the magnitude of radial velocity fluctuates slightly stronger than Model-BM, but the influence is relatively minor.

3.5 Flow Around Volute Tongue

The passage flow is significantly perturbed by the volute tongue, as suggested by the drastic variation of instantaneous static pressure and radial velocity. This section focuses the flow around the volute tongue. Three monitors, named monitor-D1/D2/D3, are set on the volute tongue at Z=±108mm, as shown in Fig. 21. The monitor-D1 is located on the interior surface of the volute tongue, and monitor-D3 is at the exit of the volute tongue, experiencing the outflow.

The temporal variation of static pressure is presented in Fig. 22. The magnitude fluctuates around the mean value. In general, the static pressure is the largest on monitor-D3 closest to the fan outlet, due to the pressure recovery, and the smallest for monitor-D1 since the flow

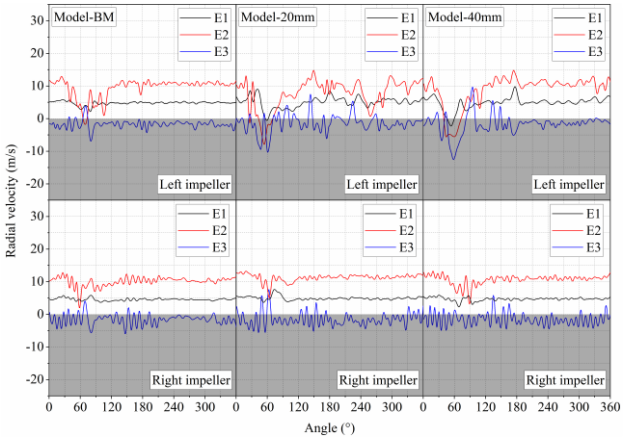

(a) monitor-E1/E2/E3

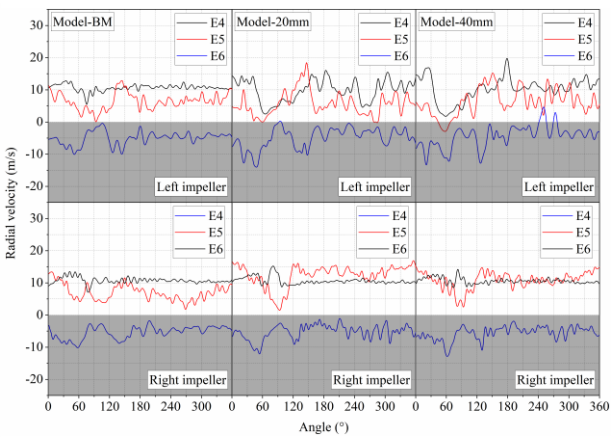

(b) monitor- E4/E5/E6

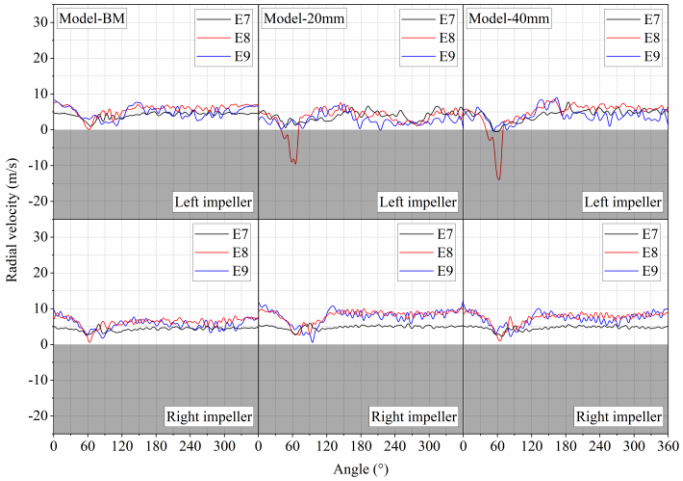

(c) monitor-E7/E8/E9

Fig. 20 Time history of radial velocity for one impeller revolution

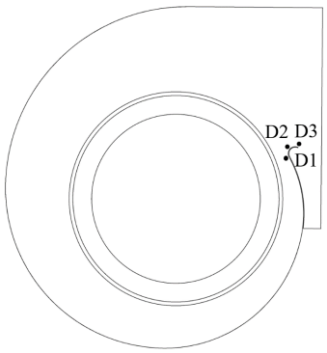

Fig. 21 Positions of the monitors on the volute tongue

leaving the impeller re-enters the gap without pressure recovery. For Model-BM, the static pressure fluctuation is minor except for monitor-D2 in the left half fan. The strong fluctuation is attributed to the asymmetric flow in the inflow cavities, where the impeller rotation imposes perturbation on one side.

The static pressure exhibits a strong and periodic fluctuation on monitors in the left half fan, while it does not show a noticeable variation in the right half fan. The fluctuating amplitude of monitor-D1 is the smallest since it is placed within the volute; however, it is interesting to notice that the fluctuating amplitude of monitor-D3 is similar to that of monitor-D2 for the Model-20mm fan, and even smaller for the Model-40mm fan. The weaker fluctuation on monitor-D3 is induced by the pressure recovery at the fan outlet and the minor influence from the impeller-volute tongue interaction. The flow leaving the impeller impinges on monitor-D2; thus, the static pressure is determined by the varied separated vortices in the blade passages and rotor-stator interaction, as presented in Fig. 17.

To quantify the motor blockage effect on flow around the volute tongue, the time-averaged and RMS fluctuation value of static pressure are listed in Table 6 and

Table **7**, respectively. The time-averaged static pressure increases from monitor-D1 to monitor-D3. As the left inlet of the fan is blocked by the motor, the mean pressure in both sides of the fan is close at monitor-D1; however, it is notably decreased in the left half fan compared with that in the right half for monitor-D2 and monitor-D3 where the outflow of the fan is affected. The difference is more considerable as the motor is placed closer to the fan inlet, i.e., for the Model-20mm fan, and is relatively small for the Model-40mm fan. The fluctuating static pressure quantifies the unsteadiness of local flow around the volute

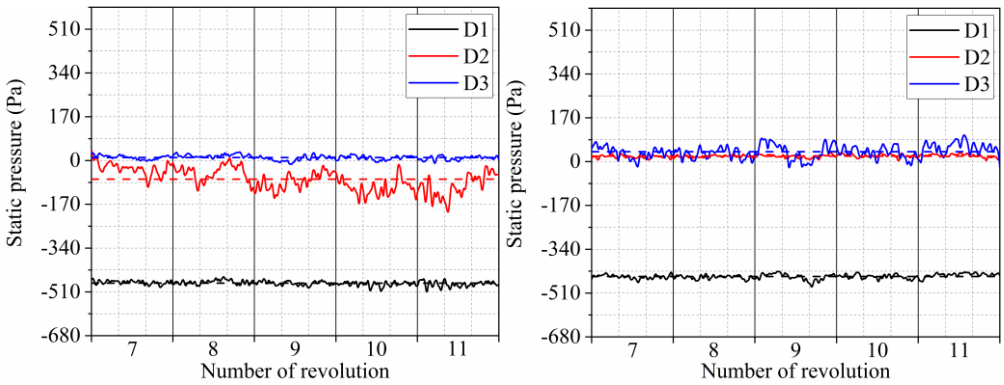

(a) Model-BM

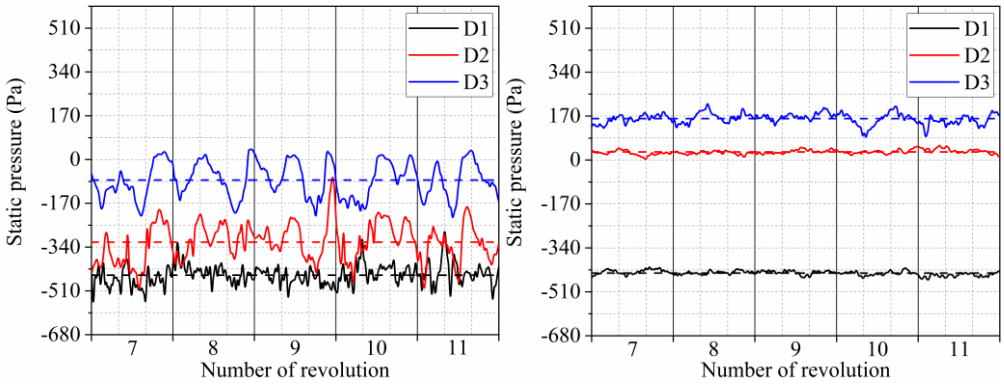

(b) Model-20mm

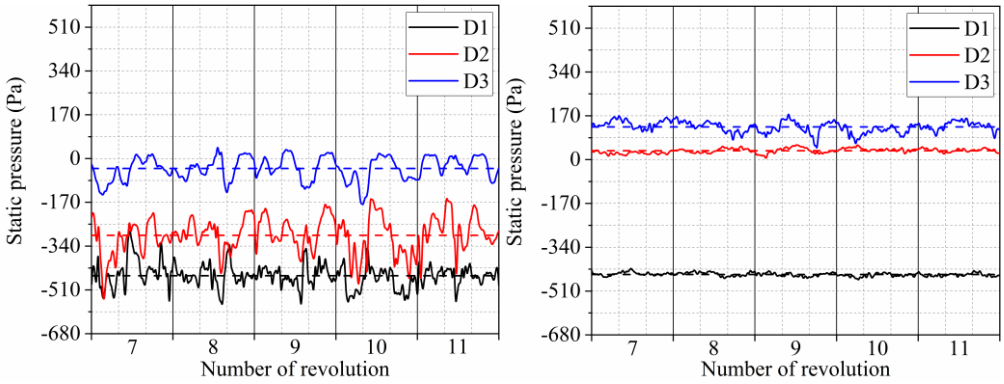

(c) Model-40mm

Fig. 22 Time history of static pressure on the volute tongue. The left sub-figures for the left half fan; the right sub-figures for the right half fan. The dashed line represents the time-averaged value

Table 6 Time-averaged static pressure at monitor-D1/D2/D3

Model	Model-BM		Model-20mm		Model-40mm	
	Left	Right	Left	Right	Left	Right
D1	-476.14	-445.77	-449.10	-437.43	-455.23	-445.75
D2	-72.57	20.88	-320.97	30.98	-298.33	34.24
D3	11.72	38.47	-79.51	160.03	-38.39	126.85

Table 7 The RMS value of static pressure fluctuation obtained at monitor-D1/D2/D3

Model	Model-BM		Model-20mm		Model-40mm	
	Left	Right	Left	Right	Left	Right
D1	9.53	9.70	43.36	9.15	48.27	7.30
D2	44.18	5.99	75.24	8.70	71.43	9.18
D3	9.09	25.93	70.20	21.31	46.07	22.23

Table 8 Case-II: mean static pressure rise and efficiency

Model	Model-BM		Model-20mm		Model-40mm	
	Left	Right	Left	Right	Left	Right
Static pressure rise (Pa)	304.10	309.19	182.12	289.92	261.83	315.52
Static pressure efficiency (%)	61.66%		45.25%		49.63%	

tongue. The asymmetric flow occurs for Model-BM, and the static pressure fluctuation in the two sides of the fan is different for monitor-D2 and monitor-D3. The difference is more significant for models with motor blockage. The fluctuation is always more significant for monitors in the left half fan. It is seen that for monitor-D1 and monitor-D2, the difference between the value in the two sides of the fan is relatively close for Model-20mm and Model-40mm, reflecting that the flow unsteadiness within and right at the volute tongue is hardly affected by the separating distance L. The difference of monitor-D3, i.e., at the fan outlet, is remarkably more significant for Model-20mm than Model-40mm, suggesting that the unsteadiness of outflow is intensely affected by the motor blockage.

4. INFLUENCE OF BOUNDARY CONDITION: A COMPARATIVE STUDY

The appropriate boundary condition is critical to the accurate simulation of flow in a double-suction turbo-machine. In most numerical investigations, the motor of the centrifugal fan is ignored, and the same inflow boundary condition is imposed on both inlets of the fan. The typical boundary condition is a constant gauge pressure at the fan outlet and a constant volume (or mass) flow rate at both fan inlets. This type of boundary condition is set up by assuming the same flow rate at the two inlets, and the influence of the obstacle such as the motor or the adjacent wall, is omitted. However, in some instances, such as the one investigated in this work, the imposed obstacle could not be omitted due to its remarkable influence; thus, selecting an appropriate type of boundary condition is crucial. In this section, we performed a comparative investigation on the impact of the type of boundary condition on the numerical results. Here, we used the boundary condition that was typically employed in most simulations, i.e., zero gauge pressure at the fan outlet and a constant flow rate at fan inlet (named Case-II), and compared the results with those in previous sections. which are obtained using the boundary condition of constant flow rate at the fan outlet and zero inlet static pressure (named Case-I). The difference in the numerical results demonstrates the influence of boundary conditions.

The performance quantities obtained using present type of boundary condition are given in Table 8. The flow rate is the same at the two inlets and is not presented here. Compared with Model-BM, the static pressure for the two inlets of Model-20mm and Model-40mm is notably different, which is contrary to the data in Table 3 where the magnitude is almost the same. The different static pressure rise results from the same flow rate at the two inlets. In Case-I, the flow rate is low in the left inlet for models with motor, as seen in Table 3, but it is the same for Case-II. The static pressure efficiency predicted by Case-II is much lower than that of Case-I, with an under-prediction of 9.42% and 8.45% for the Model-20mm and Model-40mm fans, respectively. Although there is a 2.46% difference for Model-BM, the above difference confirms the influence of the type of boundary condition on the fan performance. The temporal variation of static pressure at the two inlets is shown in Fig. 23. Compared with Fig. 6, the pressure fluctuation for Case-II is more stochastic especially for the Model-20mm and Model-40mm fans, with a noticeable high-frequency fluctuation component, which is not observed for Case-I.

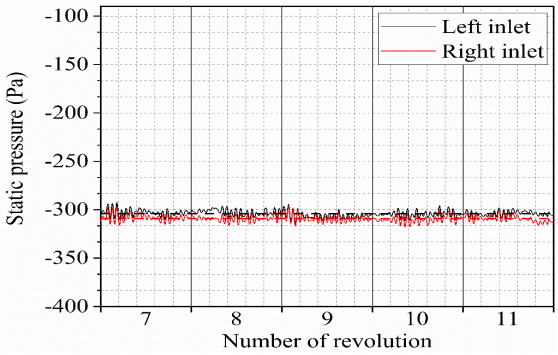

(a) Model-BM

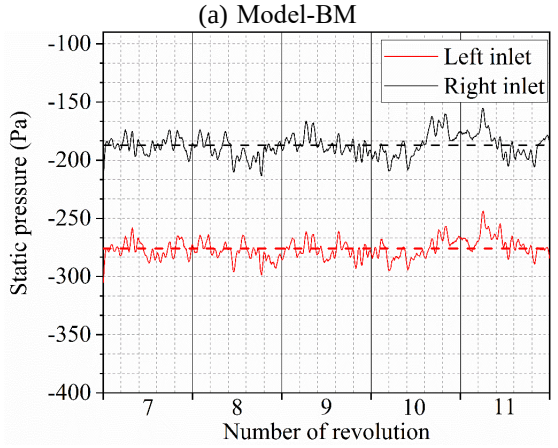

(b) Model-20mm

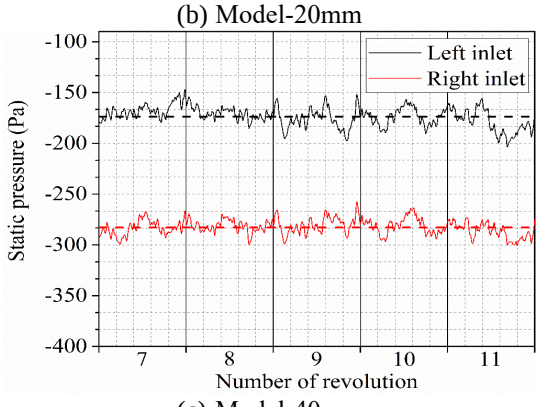

(c) Model-40mm

Fig. 23 Case-II: time history of static pressure at both fan inlets

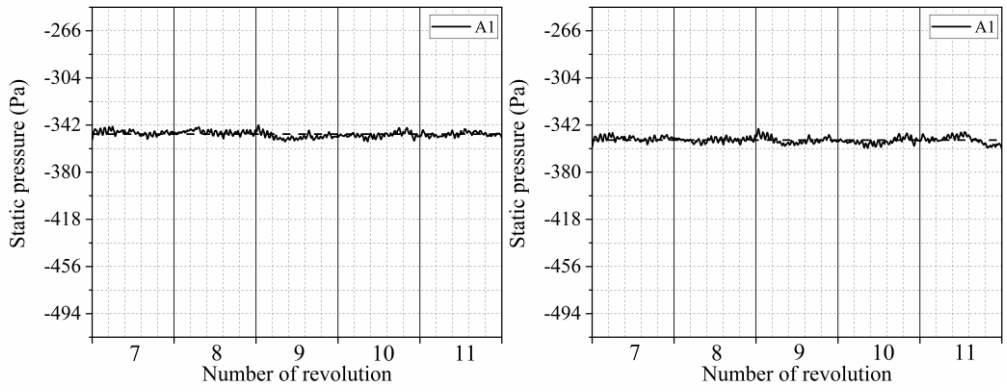

(a) Model-BM

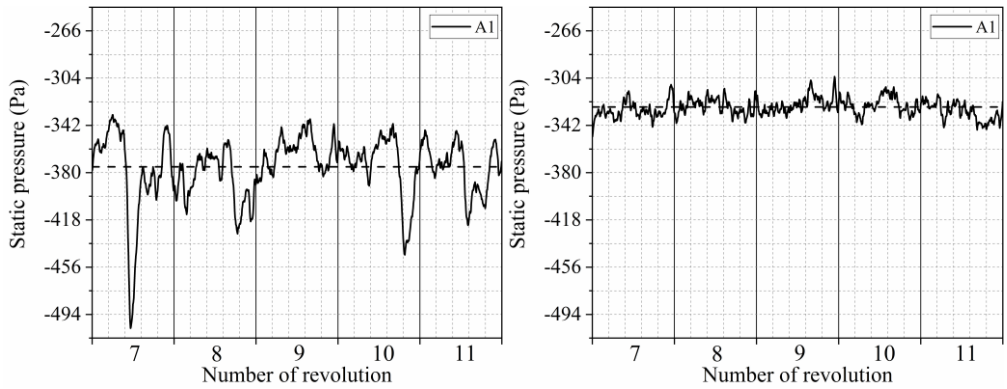

(b) Model-20mm

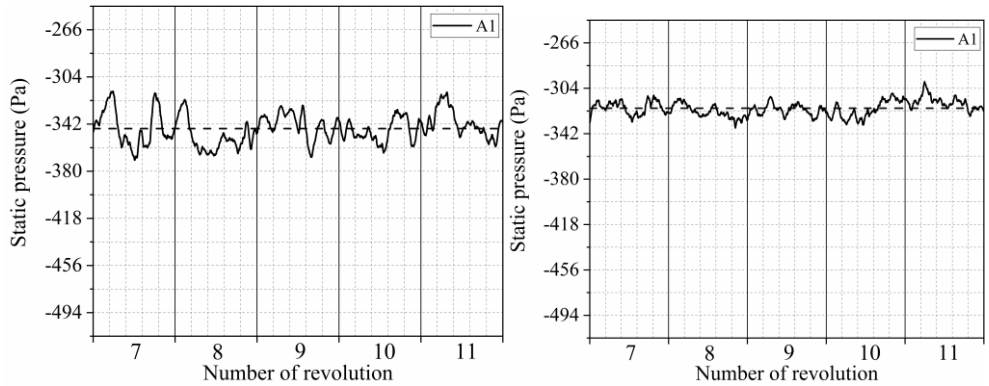

(c) Model-40mm

Fig. 24 Case-II: time history of static pressure at monitor-A1. The left sub-figures for the left half fan; the right sub-figures for the right half fan

The static pressure recorded at monitor-A1 in Fig. 24 further demonstrates the transient inflow pattern. The static pressure in the right collector exhibits a weak fluctuation similar to Case-I which is shown in Fig. 12. The fluctuating amplitude of static pressure in the left collector of the Model-20mm and Model-40mm fans is much larger than the results of Case-I. The fluctuation also presents a high-frequency pattern not observed in Fig. 12.

The flow characteristics in the blade passage are analyzed by the temporal variation of characteristic quantities recorded at the monitors. The temporal variation of static pressure and radial velocity at monitor-E4/E5/E6 is exhibited in Fig. 25 and Fig. 26, as compared with those in Fig. 19b and Fig. 20b for Case-I. The time history of both quantities is similar for Case-I and Case-II except for the absolute magnitude, which is determined by the flow rate at each inlet. For the Model-20mm and Model-40mm fans with motor blockage, there is no noticeable difference between the data of Case-I and Case-II, which fluctuates with large amplitude.

It is observed from the time history of static pressure that the decreasing pressure at monitor-E4 and increasing at monitor-E5/E6 in the right impeller does not occur in a short duration but during the period as the blade passage rotates from 30° to 150°. As the blade passage leaves the volute tongue region, the static pressure fluctuation is still substantial for flow in the left impeller of Case-II. The time history of the radial velocity does not exhibit a statistically different behavior. For flow in the right impeller of Model-20mm and Model-40mm, the reversed

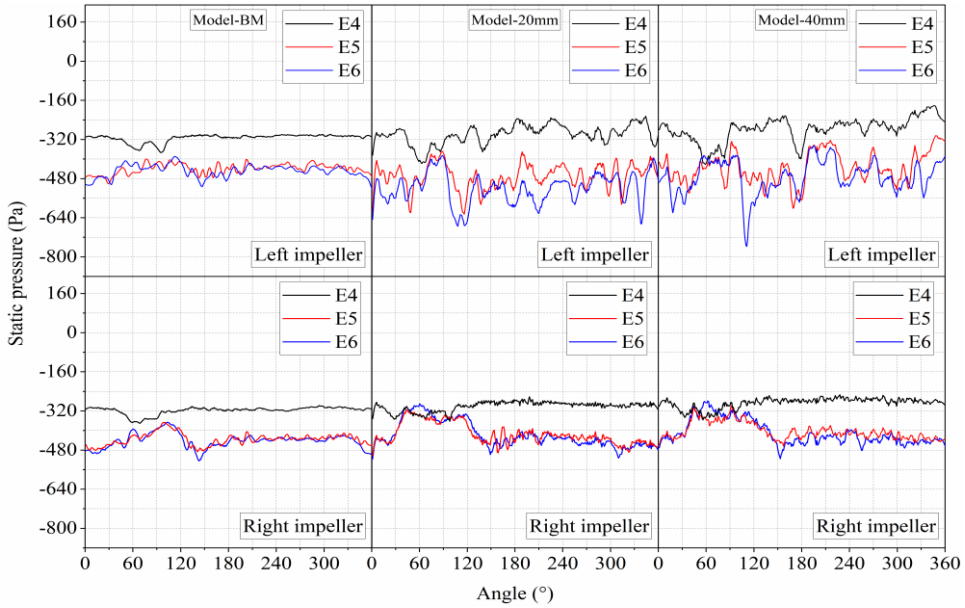

Fig. 25 Case-II: time history of static pressure for one impeller revolution

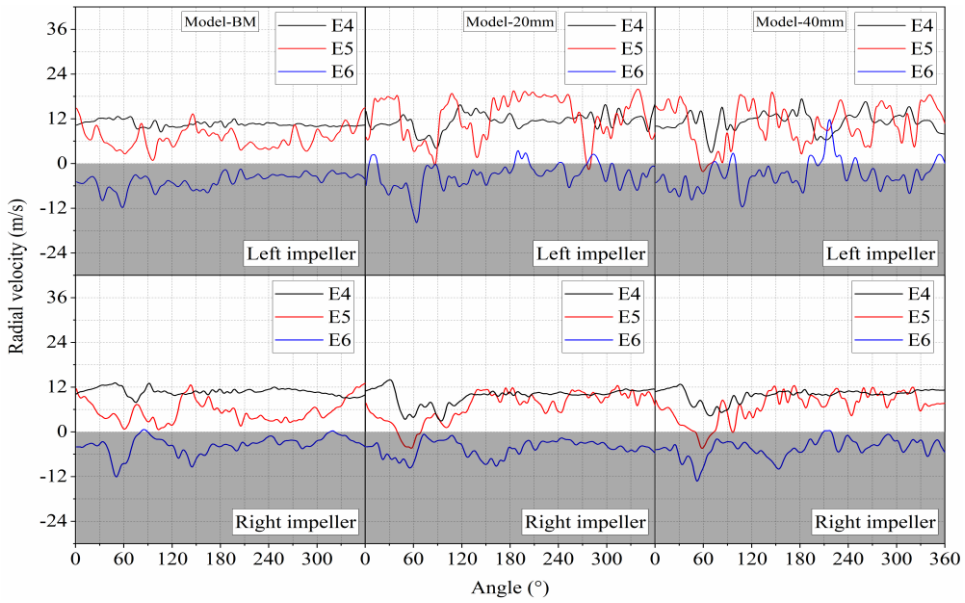

Fig. 26 Case-II: time history of radial velocity for one impeller revolution

flow occasionally occurs at monitor-E5, as the blade passage approaches the volute tongue at the circumferential position of 60°, which is not captured by the simulation of Case-I.

5.LIMITATIONS AND FUTURE WORKS

The present investigation focuses on the specific type of the double-suction centrifugal fan. The motor blockage effect is dependent on the size of the fan, especially the diameter of the collector through which the ambient air enters the fan, and the size of the motor and its distance to the adjacent collector. It is observed in the above analysis that the flow is perturbed by the motor and other perturbation sources. In applications where the fan or the motor varies in size and separating distance, the perturbation from the motor blockage may also vary and results in different transient flow patterns.

The limitation of the numerical model is also presented considering the realistic application circumstances. In some of the applications, two fans are installed in a co-axial way and are driven by the same motor placed between them. The inflow of the two fans in the in-between region interacts with each other, i.e., be perturbed in addition to the existence of the motor. In specific applications, four or even more fans could be installed in the same ventilation unit; thus, the inflow on the other side of the fan is also affected. Considering the effects of the neighboring fan, the motor's influence should be accounted for if the fluctuation of internal flow is significant.

The boundary conditions are essential in the accurate simulation of the aerodynamic performance of the fan, as

we have discussed above. We would also emphasize that in most numerical investigations, the total flow rate is fixed for a fair comparison among several fan models, and this is also the typical test methodology of the fan producers. In realistic applications, the fan inflow is affected by the blockage from the motor, the neighboring fan, and possibly the cabinet which contains the fan and the motor. The flow rate adjustment is conducted by either the valve or the fan's rotational speed. In the latter case, the flow rate is greatly affected by the motor and cabinet, which should be carefully investigated.

Future investigation should consider more influential factors in realistic engineering applications, such as the cabinet and the varying rotational speed. The type of boundary condition with atmospheric pressure at the inflow and outflow boundaries should be used to reflect the unaffected environment.

6. CONCLUSIONS

This work numerically analyzed the flow in a double-suction centrifugal fan to evaluate the influence of motor blockage on the transient characteristics of the asymmetric flow. Three models were set up, including the baseline model without consideration of the motor, and the models with the motor placed to the left of the fan with a separating distance of 20mm and 40mm. The fan performance and the transient characteristics of internal flow were analyzed in detail.

The flow rate at the left inlet blocked by the motor is reduced by 30.4% and 20.8% for the Model-20mm and Model-40mm fans, respectively, and the static pressure efficiency decreases by 9.45% and 6.04%, compared with the motor-free baseline model. It is interesting to notice that the static pressure rise is close in magnitude at the two inlets and is close to the value of the baseline model. The motor substantially perturbs the inflow at the left inlet; the static pressure highly fluctuates, and the flow in the impeller presents a disordered motion.

The motor blockage directly affects the flow at the inlet of the collector. The static pressure and radial and axial velocity do not present a circumferential uniform pattern like that of the Model-BM fan. The motor blockage significantly reduces static pressure, especially at the center of the inlet. As the inflow experiences a radial motion toward the center of the inlet cross-section, the radial velocity could be significant, either positive or negative. The inflow driven by the impeller tends to move toward the fan outlet.

The motor blockage perturbs the flow in the impeller via the mechanism of varied incidence angles due to the different flow rates and the radial motion of the inflow. For the motor blockage models, the boundary layer flow separation occurs in the region close to the fan inlet. It persists but is relatively weak in the area near the central disc, thus resulting in the degraded pressure rise. The static pressure is highly perturbed and exhibits significant fluctuation for the impeller revolution. The reversed flow in the impeller is intensified by the volute tongue confinement, especially for the Model-20mm fan, where the motor is placed close to the fan inlet. The motor highly perturbs the boundary layer flow of the volute tongue, which is significant at the tip of volute tongue and becomes weaker for outflow exiting from the fan.

A comparative study was performed to analyze the influence of boundary conditions. The conventional boundary condition, i.e., constant gauge pressure at the fan outlet and constant flow rate at the fan inlet, which is a typical choice in most simulations of flow in fans, was employed in separate simulations for all models. It was found that the conventional boundary condition under-predicts the fan efficiency, and the static pressure rise calculated at the two inlets is quite different. The passage flow exhibits more significant fluctuation than those obtained with the appropriate boundary condition, i.e., the constant flow rate at the fan outlet and constant static pressure at the inlet. It is concluded that the employment of appropriate boundary conditions is essential for accurately predicting the fan's aerodynamic performance and transient flow if the adjacent obstacles are considered.

It is finally summarized here that the motor blockage decreases the fan efficiency, but the static pressure rise is scarcely affected. The motor blockage perturbs the flow in the fan and generates strong fluctuation. The findings of this work are primarily helpful for the numerical investigations of flow in a double-suction turbomachine. For example, in the numerical aero-acoustic analysis where the perturbation is significant, and for the optimized design where the accurate prediction of the aerodynamic performance is crucial. In the engineering applications of the double-suction centrifugal fans, it is suggested that the motor, as well as other obstacles, be placed far away from the fan inlet and the motor size is better small.

ACKNOWLEDGEMENTS

The work was supported by the Natural Science Foundation of China (52176047) and the Zhejiang Province Key Research and Development Program (Grant Nos. 2022C01227 and 2022C01159).

CONFLICT OF INTEREST

The authors declare that they have no conflict of interest.

AUTHORS CONTRIBUTION

Shouhua Du: Data curation, Formal analysis, Investigation, Methodology, Software, Writing – original draft. **Xiaoming Wu:** Validation. **Zhongxian Wang:** Validation. **Wenxia Yang:** Validation. **Zhengdao Wang:** Supervision. **Wei Zhang:** Conceptualization, Formal analysis, Funding acquisition, Investigation, Project administration, Resources, Supervision, Writing – review & editing. **Zexin Yang:** Investigation.

REFERENCES

Chang, L., Yang, C., Su, X., Dai, X., Xu, Q., & Guo, L. (2024). Investigations on affinity law under gas–liquid conditions in multistage radial and mixed-

flow multiphase pumps. *International Journal of Fluid Engineering, 1*, 013503. https://doi.org/10.1063/5.0191201

Chen, Z. Y., He, H. J., Yang, H., Wei, Y. K., & Zhang, W. (2024). Asymmetric flow in a double-suction centrifugal fan induced by an inclined impeller. *Physics of Fluids, 36*, 017113. https://doi.org/10.1063/5.0178927

Chen, Z. Y., Yang, H., Wei, Y. K., He, H. J., Zhang, C. Y., Nie, T. H., Yu, P. Q., & Zhang, Wei. (2022). Effect of a radially offset impeller on the unsteady characteristics of internal flow in a double-suction centrifugal fan. *Processes*, *10*, 1-31. http://dx.doi.org/10.3390/PR10081604

González, J., Delgado, L., Velarde-Suárez, S., Fernández-Oro, J. M., Díaz, K. A., Rodríguez, D., & Méndez, D. (2020). Experimental study of the unsteady vibration signature for a Sirocco fan unit. *Journal of Low Frequency Noise, Vibration and Active Control*, *39*, 129-148. https://journals.sagepub.com/doi/10.1177/1461348419837418

González, J., Oro, J. F., Delgado, L., Méndez, D., Argüelles, K. M., Velarde-Suárez, S., & Rodríguez, D. (2019). Symmetrized dot pattern analysis for the unsteady vibration state in a Sirocco fan unit. *Applied Acoustics*, *152*, 1-12. http://dx.doi.org/10.1016/j.apacoust.2019.03.017

Gunn, E. J., Tooze, S. E., Hall, C. A., & Colin, Y. (2013). An experimental study of loss sources in a fan operating with continuous inlet stagnation pressure distortion. *Journal of Turbomachinery, 135*, 051002. http://dx.doi.org/10.1115/1.4007835

Hariharan, C., & Govardhan, M. (2016). Improving performance of an industrial centrifugal blower with parallel wall volutes. *Applied Thermal Engineering, 109*, 53-64. http://dx.doi.org/10.1016/j.applthermaleng.2016.08.045

Hariharan, C., & Govardhan, M. (2019). Aerodynamic performance and flow characteristics of an industrial centrifugal blower volute with varied cross-sectional shapes/area ratios. *International Journal of Turbo & Jet-Engines, 36*, 89-106. http://dx.doi.org/10.1515/tjj-2016-0060

Kang, D. H., Shinohara, T., Nakamura, S., Nishibe, K., Sato, K., Yokota, K., & Ohue, H. (2020). Performance degradation and flow instability of axial-flow fan due to upstream obstacle. *Journal of Fluids Engineering, 142*, 091207. http://dx.doi.org/10.1115/1.4047535

Kim, J. H., Cha, K. H., & Kim, K. Y. (2013). Parametric study on a forward-curved blades centrifugal fan with an impeller separated by an annular plate. *Journal of Mechanical Science and Technology, 27*, 1589-1595. http://dx.doi.org/10.1007/s12206-013-0404-4

Kim, J. S., Jeong, U. C., Kim, D. W., Han, S. Y., & Oh, J. E. (2015). Optimization of Sirocco fan blade to reduce noise of air purifier using a metamodel and evolutionary algorithm. *Applied Acoustics, 89*, 254-266.http://dx.doi.org/10.1016/j.apacoust.2014.10.005

Li, D. (2021). Design for new type centrifugal fan and passageway of the air conditioner indoor unit. *IOP Conference Series: Earth and Environmental Science, 632*, 052003. http://dx.doi.org/10.1088/1755-1315/632/5/052003

Li, W. (2024). Effects of interface model on performance of a vortex pump in CFD simulations. *International Journal of Fluid Engineering, 1*, 013901. https://doi.org/10.1063/5.0196213

Li, Z. H., Luo, P., Zhu, M. J., Chen, Z. Y., Liu, Y., & Li, G. H. (2023). Effect of motor installation heights on the performance of an isolated centrifugal fan. *Processes*, *11*, 2116. http://dx.doi.org/10.3390/PR11072116

Lin, S., & Chou, C. (2004). Blockage effect of axial-flow fans applied on heat sink assembly. *Applied Thermal Engineering, 24*, 2375–2389. https://doi.org/10.1016/j.applthermaleng.2004.03.009

Liu, P., Shiomi, N., Kinoue, Y., Jin, Y. Z., & Setoguchi, T. (2012). Effect of inlet geometry on fan performance and flow field in a half-ducted propeller fan. *International Journal of Rotating Machinery,* 463585. http://dx.doi.org/10.1155/2012/463585

Liu, Z. F., Yang, H., He, H.J., Yu, P. Q., Wei, Y. K., & Zhang, W. (2022). Flow instability in a volute-free centrifugal fan subjected to non-axisymmetric pre-swirl flow from upstream bended inflow tube. *Proceedings of the Institution of Mechanical Engineers, Part A: Journal of Power and Energy, 236*, 689-713. http://dx.doi.org/10.1177/09576509211062664

Lun, Y. X., Ye, X. X., Lin, L. M., Ying, C. L., & Wei, Y. K. (2019). Unsteady characteristics of forward multi-wing centrifugal fan at low flow rate. *Processes, 7*, 691-691. http://dx.doi.org/10.3390/pr7100691

MacDonald, M. A., Gullbrand, J., Nishi, Y., & Baugh, E. (2009). Notebook blower inlet flow and acoustics: experiments and simulations. *Noise Control Engineering Journal, 57*, 348-348. https://doi.org/10.3397/1.3151971

Madhwesh, N., Vasudeva, K. K., & Yagnesh, S. N. (2018). Effect of innovative circular shroud fences on a centrifugal fan for augmented performance - A numerical analysis. *Journal of Turbomachinery, 32*, 185-197.http://dx.doi.org/10.1007/s12206-017-1220-z

More, K. C., Dongre, S., & Deshmukh, G. P. (2019). Experimental and numerical analysis of vibrations in impeller of centrifugal blower. *SN Applied Sciences, 2*, 7-11.http://dx.doi.org/10.1007/s42452-019-1853-x

Motohiko, A., Tsuneaki, I., & Tomio, O. (2003). PIV measurement and numerical prediction of flow around a fan. *Journal of the Visualization Society of Japan, 23*, 203-206. http://dx.doi.org/10.3154/JVS.23.SUPPLEMENT1_203

Nilugal, M. L., Karanth, K. V., & Madhwesh, N. (2022). Numerical investigations on the effect of volute casing treatment for performance augmentation in a centrifugal fan. *Proceedings of the Institution of Mechanical Engineers, Part C: Journal of Mechanical Engineering Science, 236*, 2791-2802. http://dx.doi.org/10.1177/09544062211034190

Pathak, Y. R., Deore, K. D., & Ozarkar, R. R. (2020). Effect of impeller parameters on the flow inside the centrifugal blower using CFD. *International Journal of Recent Technology and Engineering, 8*, 3977-3980. http://dx.doi.org/10.35940/ijrte.f8973.038620

Patil, S. R., Chavan, S. T., Jadhav, N. S., & Vadgeri, S. S. (2018). Effect of volute tongue clearance variation on performance of centrifugal blower by numerical and experimental analysis. *Materials Today: Proceedings, 5*, 3883-3894. http://dx.doi.org/10.1016/j.matpr.2017.11.643

Qin, H. J., Wang, Z.D., He, H.J., Yang, W. X., Wang, Z.X., Zhu, Z. C., & Zhang, W. (2023). Effect of motor intrusion on the aerodynamic performances and unsteady characteristics of internal flow of a volute-free centrifugal fan. *Proceedings of the Institution of Mechanical Engineers, 237*, 729-746. http://dx.doi.org/10.1177/09576509221144212

Rong, L., Bohle, M., & Gu, Y. (2024). Improving the hydraulic performance of a high-speed submersible axial flow pump based on CFD technology. *International Journal of Fluid Engineering, 1*, 013902. https://doi.org/10.1063/5.0191683

Sui, D., Wang, S. S., Mao, J. R., Kim, T. & Lu, T. J. (2009). Exit flow behavior of axial fan flows with/without impingement. *Journal of Fluids Engineering, 131*, 061103. http://dx.doi.org/10.1115/1.3130246

Tsurusaki, H., & Kinoshita, T. (2001). Flow control of rotating stall in a radial vaneless diffuser. *Journal of Fluids Engineering*, *65*, 1133-1151. http://dx.doi.org/10.1115/1.1351174

Wang, C., Mai, K., Fang, L. H., & Liu, N. T. (2021). Aerodynamic design and acoustic effect study of key geometric parameters of a Sirocco fan. *Noise Control Engineering Journal*, *69*, 431-450. https://doi.org/10.3397/1/376940

Zhang, W. Q., & Vahdati, M. (2019). A parametric study of the effects of inlet distortion on fan aerodynamic stability. *Journal of Turbomachinery ,141*, 011011. http://dx.doi.org/10.1115/1.4041376

Zhao, X. T., & Guan, J. H. (2023). *Influence of the spatial position of the semi-open impeller on the internal flow field in centrifugal fans.* Journal of Physics: Conference Series, 2574. https://iopscience.iop.org/article/10.1088/1742-6596/2574/1/012007

Zheng, S. H., Shao, Z. H., Liu, J. F., Chen J. X., Li, Y. L., & Chai, M. (2023). Flow characteristics of a centrifugal fan with optimized edge curvatures of an impeller front disk. *Proceedings of the Institution of Mechanical Engineers, 237*, 916-928. https://journals.sagepub.com/doi/10.1177/09576509231154950

Zhou, W. Q., Zhou, P. J., Xiang, C., Wang, Y., Mou, J. G., & Cui, J. Y. (2023). A review of bionic structures in control of aerodynamic noise of centrifugal fans. *Energies*, *16*, 4331. http://dx.doi.org/10.3390/EN16114331